Bioconjugate Chemistry

Article

Combretastatin A-4 Analogue: A Dual-targeting and Tubulin Inhibitor Containing Antitumor Pt(IV) Moiety with a Unique Mode of Action

Xiaochao Huang, Rizhen Huang, Shaohua Gou, Zhi-xin Liao, Heng-Shan Wang, and Zhimei Wang

Bioconjugate Chem., **Just Accepted Manuscript** • DOI: 10.1021/acs.bioconjchem.6b00353 • Publication Date (Web): 05 Aug 2016

ACS Publications

Bioconjugate Chemistry is published by the American Chemical Society. 1155 Sixteenth Street N.W., Washington, DC 20036

Combretastatin A-4 Analogue: A Dual-targeting and Tubulin Inhibitor Containing Antitumor Pt(IV) Moiety with a Unique Mode of Action

Xiaochao Huang[1], [†, ‡] Rizhen Huang[1], [†, ‡] Shaohua Gou,[†, ‡*] Zhimei Wang [†, ‡], Zhixin Liao,[†, ‡] and Hengshan Wang[§, *]

[†]Pharmaceutical Research Center and School of Chemistry and Chemical Engineering, Southeast University, Nanjing 211189, China

[‡]Jiangsu Province Hi-Tech Key Laboratory for Biomedical Research, Southeast University, Nanjing 211189, China

[§]State Key Laboratory for the Chemistry and Molecular Engineering of Medicinal Resources (Ministry of Education of China), School of Chemistry and Pharmaceutical Sciences of Guangxi Normal University, Guilin 541004, China

Supporting Information

Table of Contents Graphic

TOC

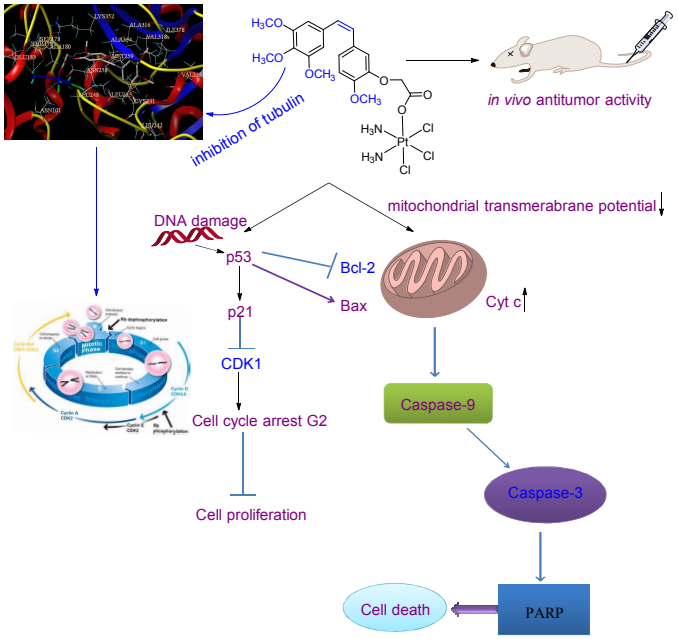

ABSTRACT: Three new Pt(IV) complexes comprising a combretastatin A-4 analogue were designed and synthesized. The resulting antitumor Pt(IV) complexes could significantly improve the anti-proliferative activity and overcome the drug resistance of cisplatin in vitro. Interestingly, these novel compounds can not only carry the DNA binding Pt(II) warhead into the cancer cells but also have a small molecule fragment that can inhibit tubulin polymerization. Among them, complex **13,** which was attached to an inhibitor of tubulin at one axial position of Pt(IV) octahedral coordination sphere, could effectively enter cancer cells, arrest the cell cycle in HepG-2 cancer cells at G2/M phases, and induce activation of caspases triggering apoptotic signaling via the mitochondrial-dependent apoptosis pathways. Moreover, complex **13** has the ability of effectively inhibiting the tumor growth in the HepG-2 xenograft model without causing significant loss of animal body weight in comparison with cisplatin.

INTRODUCTION

Platinum(II) based complexes, including cisplatin, carboplatin and oxaliplatin (**Figure 1**), are the most frequently applied DNA-damaging anticancer drugs, and among them cisplatin is the first-line chemotherapeutic agent against certain types of malignancies.[1-7] Nevertheless, the effectiveness of Pt(II) drugs has been heavily limited by high toxicity, severe side effects and inherent or acquired drug resistance.[8-11] Therefore, great efforts have been devoted to the design of novel platinum based drugs with improved therapeutic properties, clinical efficacy and without acquired resistance. [12-15]

Recent studies have described the combination of platinum anticancer agents with inhibitors of tubulin, primarily with paclitaxel and docetaxel, resulting in the improvement of therapeutic efficacy.[16] The inhibitors of tubulin, such as the natural products vinblastine, vincristine, paclitaxel and docetaxel,[17,18] are forceful as anti-mitotic agents that can induce tumor cells apoptosis and inhibit cancer cells proliferation and angiogenesis. Microtubules are well known key components of the cytoskeleton which is composed of α, β-tubulin heterodimers, playing a significant role in a variety of essential cellular processes, notably mitotic spindle assembly during cell division, cell proliferation, intracellular transport, cell signaling, and migration.[19-21] Meanwhile, inhibition of the assembly of tubulin into microtubules, or inversely, the depolymerization of microtubules leading to the arrest of cell division and eventually to apoptosis, makes the microtubule cytoskeleton an effective and attractive molecular target for cancer chemotherapeutic agents. Combretastatin-A4 (CA-4, **Figure 2**), as a natural cis-stilbene product, isolated

from the bark of African willow tree *Combretum caffrum*, is one of the well known tubulin-binding molecules that strongly inhibit tubulin polymerization by binding to the colchicine binding site, causing rapidly vascular shutdown and cell death in tumor cells. CA-4 has shown strong cytotoxicity against a large number of human cancer cells, including those that are multidrug resistant ones.[22-26] Particularly, Pt(II) complexes comprising a CA-4 analogous chalcone seemed to primarily target the tubulin at a physiologically meaningful concentrations.[27] Hence, a combination of cytotoxic DNA damaging agents, such as platinum drugs, with inhibitor of tubulin can be a fascinating strategy for targeting microtubules, and at least in theory, can enhance the efficacy and overcome the resistance of the platinum drugs. However, the activities of these compounds, which hinge on the intracellular aquation of the Pt(II) complexes to release the inhibitor of tubulin, were not as potent as expected. Furthermore, it is extremely difficult to control major obstacles in administering free-drug formulations, such as the definitive exposure to the targets of interest, individual pharmacokinetics, or bio-distribution parameters, when drugs are individually administered.

Rather than depend on aquation for the synchronous release of two anti-tumor drugs inside the cancer cells, it might be an alternative way to construct a single prodrug which takes advantage of the favorable chemical properties of Pt(IV) complexes towards that end. Recently, there have been several reports on Pt(IV) prodrugs derived from cisplatin or oxaliplatin with chalcone derivatives or phenylbutyrate as the axial ligands in the octahedral geometry of Pt(IV) complexes, in which the Pt(IV) compounds were reduced

to Pt(II) equivalents in the tumor cells and released other molecular fragments to activate p53, suppress efficacy of histone deacetylases (HDACs) and induce cell cycle arrest at S phase and cell death through apoptosis, respectively.[28-30] However, hitherto, no examples of a prodrug containing both cisplatin and combretastatin-A4 (CA-4) has been reported as a inhibitor of tubulin polymerization. In recent years, the work of Hsieh and Nam showed that 3,4,5-trimethoxy substitution on the A-ring and the cis-orientation were essential for efficient CA-4 inhibition of tubulin polymerization and antitumor activities.[31,32] In this mind, we designed and tried to obtain a novel dual-targeting platinum(IV) anticancer prodrug with the ability to release cisplatin and CA-4 analogue for their respective biological actions that can not only carry the DNA binding platinum warhead into the tumor cells but also have a small molecule fragment that can inhibit tubulin polymerization **(Figure 3.)**.

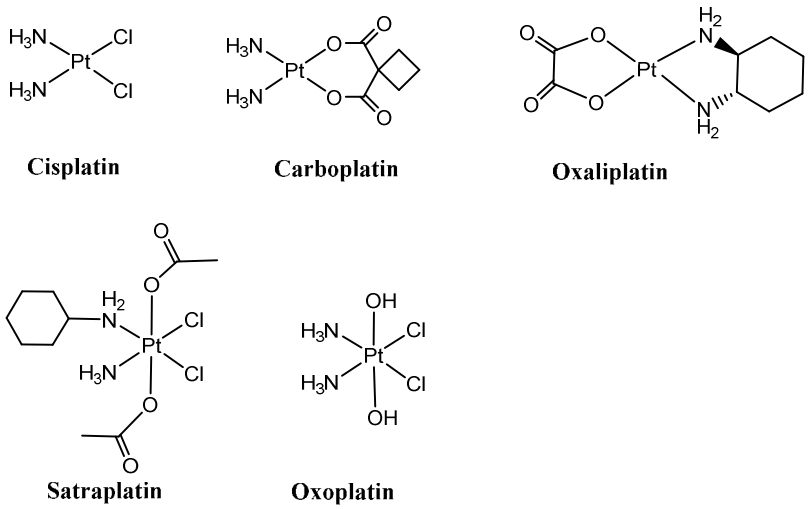

Figure 1. FDA approved platinum(II) anticancer agents, platinum(IV) prodrug in clinical trials, satraplatin, and platinum(IV) compound commonly used as precursor for acylation

reactions, oxoplatin.

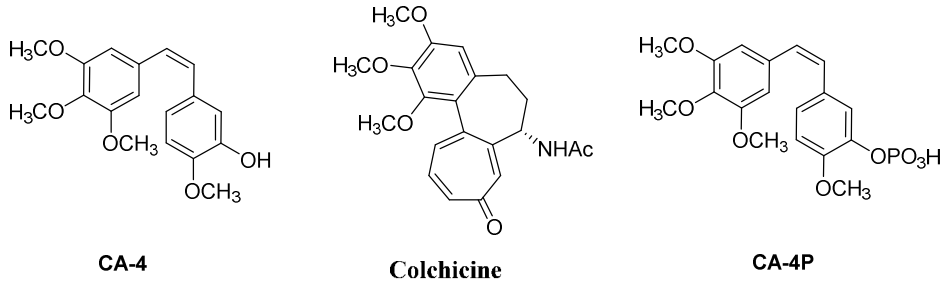

Figure 2. Structures of natural products and clinical trial agent (CA-4P) that bind at the colchicine-binding site of tubulin.

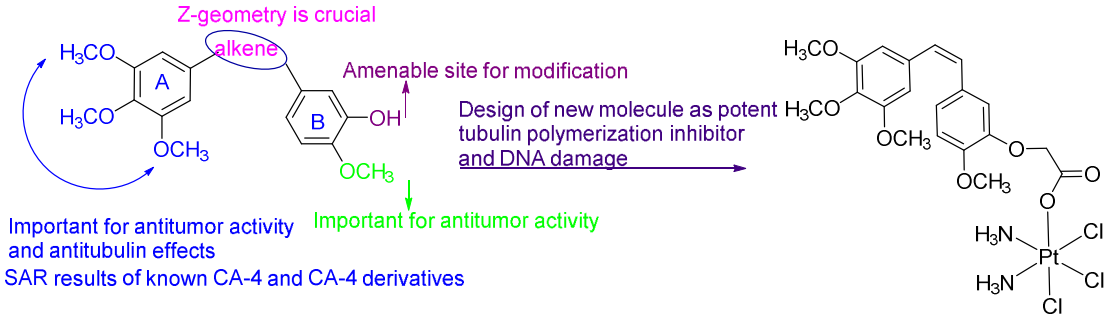

Figure 3. Design of a novel platinum(IV) prodrug as a potential anti-tubulin and anti-tumor agent.

RESULTS AND DISCUSSION

Synthesis and Characterization. The CA-4 analogue were synthesized according to the reported procedures.[33-35] Platinum(IV) precursor complexes were synthesized according to the reported procedure.[36] Target compounds purity was determined by microanalysis and their structures were characterized by HR-MS, ^{1}H and ^{13}C NMR spectrometry. The synthetic profiles of the compounds and their chemical structures are listed in **Schemes 1** and **2**.

Scheme 1. Synthetic Pathway to Target Compounds 10-12. Reagents and Conditions:

(a) H_2O, rt

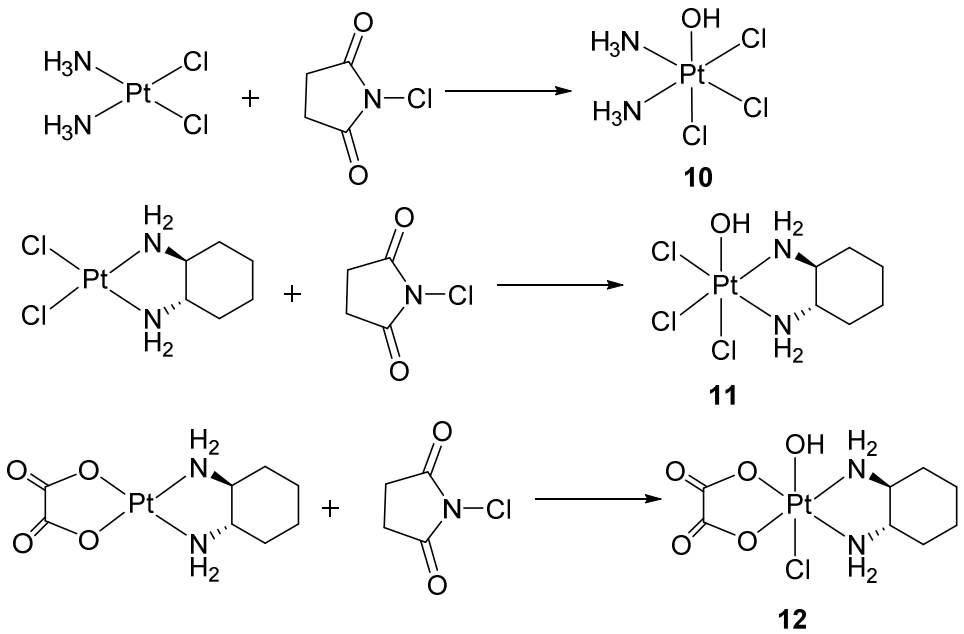

Scheme 2. Synthetic Pathway to Target Compounds 13-15. Reagents and Conditions: (a) $NaBH_4$, CH_3OH, 0 ^oC; (b) PBr_3, CH_2Cl_2, 0 ^oC; (c) PPh_3, toluene, 110 ^oC (d) NaH, DCM, rt; (e) 1N HCl/CH_3OH, 50 ^oC; (f) K_2CO_3, DMF, rt.; (g) LiOH.H_2O, THF/H_2O, rt.; (h) TBTU, Et_3N, DMF, rt.

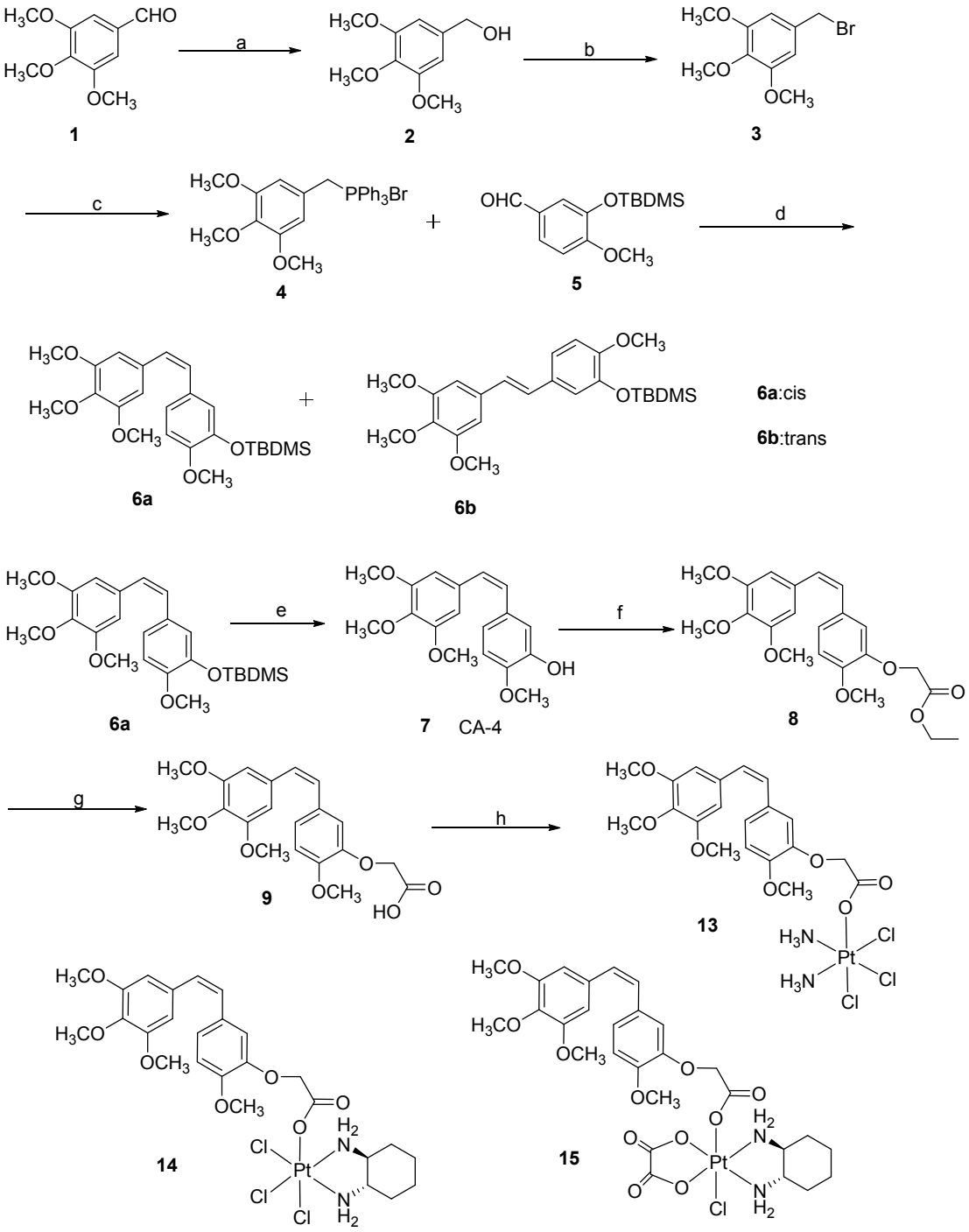

HPLC Analyses On the Pt(IV) Complexes Released Ability. To investigate whether the activities of the synthetic Pt(IV) complexes were released Pt(II) equivalents as planned under reduction, complex **13** in a solution of acetonitrile and water (1.5:1) to release compound **9** and cisplatin under reduction with ascorbic acid was studied by

HPLC. As shown in **Figure S1**, complex **13** was gradually reduced to release compound **9** and cisplatin as the time passed, accompanied by the falling down peak of complex **13** and the rising peak of compound **9**. It was noted in the HPLC chromatograms that cisplatin was not observed due to its weak chromophore under the ultraviolet detecting condition. Since oxaliplatin could be observed under the ultraviolet detecting condition, we further investigated the behavior of Pt(IV) complex **15** under the same condition. As illustrated in **Figure S1**, similar trend was observed. These results suggested that the Pt(IV) complexes were easily reduced to their Pt(II) equivalents in the presence of ascorbic acid at the room temperature, implying its potential biological activity.

In Vitro Cytotoxicity Assay. The cytotoxicity of target complexes were first screened in vitro against five different human cancer cell lines representative of MCF-7 (breast), HCT-116 (colon), HepG-2 (hepatoma), Bel-7404 (hepatoma), NCI-H460 (lung) and LO2 (human normal liver cell line) with cisplatin, oxaliplatin, DACHPt and CA-4 as reference controls using MTT assay. The corresponding IC_{50} values obtained after 72 h exposure, are summarized in Table 1. As shown in Table 1, the compound CA-4 analogue **9** showed a low cytotoxicity against the tested tumor cell lines than positive drug CA-4. However, compounds **13-15,** the Pt(IV) derivatives of cisplatin, oxaliplatin, or DACHPt with one CA-4 analogue ligand in the axial position, exhibited significant antitumor activity against all tested cell lines. The Pt(IV) derivative of cisplatin, complex **13**, was significantly more potent than the commercial anticancer drug cisplatin with IC_{50} values in the range of 0.35–3.01 μM, and simultaneously showed low cytotoxicity against LO2 cells with IC_{50} value of 36.06±3.21 μM compared with the positive drug cisplatin

(3.54±0.26 μM) and CA-4 (0.58±0.11 μM), respectively, making it as a good antitumor drug candidate. The Pt(IV) derivatives of DACHPt and oxaliplatin, complexes **14** and **15**, displayed better cytotoxicity against the tested cell lines than their references DACHPt and oxaliplatin, with IC_{50} values in the range of 0.87–5.95 and 4.69–9.53 μM, respectively. Especially, both **14** and **15** also exhibited low cytotoxicity against LO2 cells with IC_{50} values of 37.84±2.25 and 38.84±2.23 μM compared with DACHPt (2.66±0.23, μM) and oxaliplatin (4.71±0.41 μM), respectively.

Table 1. Effect of Target Compounds against Cell Viability of Different Cell Lines

Compd.	IC_{50} (μM)					
	MCF-7	HepG-2	HCT-116	Bel-7404	NCI-H460	LO2
9	25.21±2.18	11.79±0.84	27.29±2.43	15.59±0.54	12.56±0.57	48.42±2.92
13	2.14±0.15	0.35±0.11	3.01±0.27	2.17±1.56	0.56±1.19	36.06±3.21
14	4.43±0.45	0.87±0.71	3.89±0.42	5.95±1.03	0.91±1.85	37.84±2.25
15	9.53±0.87	6.89±0.52	4.89±0.51	8.94±0.15	4.69±0.23	38.84±2.23
CA-4	0.13±0.13	0.23±0.13	0.25±0.17	1.16±0.35	0.33±0.15	0.58±0.11
CDDP [a]	5.90±0.35	3.96±0.28	7.78±0.63	12.47±0.49	18.93±1.08	3.54±0.26
OXP [b]	10.73±0.89	21.65±1.78	3.98±0.26	17.90±2.01	14.36±1.25	4.71±0.41
DACHPt [c]	24.46±1.95	21.47±2.53	8.18±0.74	20.75±1.75	19.51±1.81	2.66±0.23

[a]Cisplatin, [b]Oxaliplatin, [c]Dichloro(trans-1,2-diaminocyclohexane)platinum.

Notably, complex **13** showed up to 11.3-fold increased cytotoxicity compared with

cisplatin in HepG-2 cells and exhibited almost similar antitumor activity to CA-4. The similar trend was also observed in NCI-H460 cells. This Pt(IV) compound showed high potency against the tested cancer cell lines, which can be due to the "synergistic accumulation" of both the Pt moiety and the CA-4 analogue **9**, respectively. Interestingly, all resulting Pt(IV) complexes displayed low cytotoxicity than their corresponding positive controls (cisplatin, oxaliplatin and DACHPt) against human normal LO2 cell line, indicating that these complexes have a selective toxicity for the tumor cells over the normal cell.

Table 2. In Vitro Growth Inhibitory Effect of Selected Compounds 13-15 on Cisplatin-Resistant Cell Lines SGC-7901 and A549

Compd.	IC_{50} (μM)		resistant factor [d]	IC_{50} (μM)		resistant factor [d]
	SGC-7901	SGC-7901/CDDP		A549	A549/CDDP	
9	58.93±5.26	61.15±5.26	1.04	21.36±0.58	29.68±0.71	1.44
13	0.89±0.07	1.62±0.09	1.82	2.04±0.92	2.77±1.66	1.36
14	3.98±0.28	7.91±1.24	1.99	2.93±0.47	8.47±1.52	2.89
15	7.37±0.62	9.53±0.87	1.29	5.56±1.53	10.38±1.35	1.87
CA-4	84.54±6.69	77.68±5.23	-	0.18±0.49	2.68±0.31	14.89
CDDP [a]	1.11±0.09	12.86±0.73	11.58	6.29±1.59	25.33±0.73	4.03
OXP [b]	15.21±1.03	21.65±1.78	1.42	9.81±0.82	32.54±0.97	3.32
DACHPt [c]	12.36±1.07	21.47±2.53	1.74	8.37±0.36	30.41±1.34	3.63

[a]Cisplatin, [b]Oxaliplatin, [c]Dichloro(trans-1,2-diaminocyclohexane)platinum, [d]The values express the ratio between IC_{50} determined in resistant and nonresistant cell lines.

Effects of Complexes 13-15 on Drug Resistant Cell Lines. Drug resistance is a

critical therapeutic problem that limited the efficacies of cisplatin for a variety of human cancer cells. According to the above biological result, we further evaluated sensitivity to the selected complexes (**13-15**) of two cisplatin resistant and non-resistant cancer cells (SGC-7901 human gastric cancer cell lines) and human lung epithelial cells (A549). As shown in Table 2, the IC_{50} values of cisplatin against SGC-7901/CDDP and A549/CDDP resistant cell lines were increased to 12.86 and 25.33 μM, respectively. Interestingly, the activity of compound **13** was not markedly changed for these two cisplatin resistant cancer cell lines compared with the sensitive ones, its IC_{50} values against cisplatin resistant SGC-7901 and A549 cell-lines were 1.62 and 2.04 μM, respectively. It was of much significance to observe that compound **13** had a much lower resistance factor (1.82 for resistant SGC-7901 cell line and 1.36 for resistant A549 cell line) than cisplatin (11.58 for resistant SGC-7901 cell line and 4.03 for resistant A549 cell line). Moreover, **15** and **14** have potent cytotoxicity against parental cells and cells resistant to cisplatin comparable to that of oxaliplatin and DACHPt, and have smaller resistant factors, suggesting that these compounds might be useful in the treatment of drug refractory tumors resistant to other platinum drugs.

Cellular Uptake. Since complexes **13** and **14** exhibited better cytotoxicity, they were selected to carry out the cellular uptake test in HepG-2 cells by using the inductively coupled plasma mass spectrometry (ICP-MS). As shown in **Figure 4** and Table 3, treating HepG-2 cells with the complexes (10.0 and 20.0 μM) for 12 h resulted in a substantial increase in the content of cellular platinum in a concentration dependent manner,

suggesting facile internalization of the complexes within 12 h. Particularly, the uptake of complex **13** was significantly higher than those of cisplatin and complex **14**. After exposure to 20.0 μM of complex **13** for 12 h, the concentration of cellular platinum rose to 606 ng/10^6 cells, which is nearly two times as much as that of cisplatin. Upon the results from the cytotoxicity assay and cellular uptake tests, it seems that there might be a positive correlation between these two tests, namely, the enhanced cellular uptake can result in the increase of the cytotoxicity. However, the platinum accumulation of complex 14 on the tested cells was not always high in comparison with cisplatin, which did not correlate with the cytotoxicity against HepG-2 cells. The un-correlation between the intracellular platinum levels and the cytotoxicity of complexes may be due to the fact that the intracellular platinum level is, although important, not the only factor deciding the cytotoxicity of the complexes.

Table 3. Cellular Uptake of 13 and 14 in HepG-2 Cells after 12 h of Incubation

Complex	Pt content (ng/10^6 cells)
	HepG-2
13 (10 μM/L)	235±21
13 (20 μM/L)	606±61
14 (10 μM/L)	140±12
14 (20 μM/L)	220±19
CDDP (10 μM/L)	157±21
CDDP (20 μM/L)	351±18

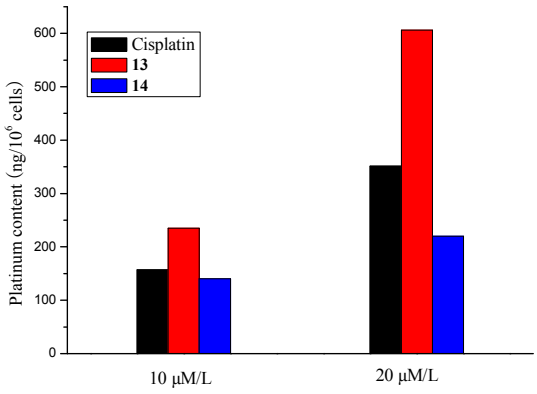

Figure 4. Intracellular accumulation of cisplatin, **13** and **14** (10, 20 μM) in HepG-2 cells after 12 h. Each value shown in the table is in nanograms of platinum per 10^6 cells. Results are expressed as the mean ± SD for three independent experiments.

Effects of complex 13 on Tubulin Polymerization in vitro. Microtubule perturbing agents can either enhance or inhibit the assembly of microtubules. It is well-known that the mechanism of tubulin-binding agents can be divided into two types: stimulating agents (e.g. paclitaxel) and inhibiting agents (e.g. CA-4).[37] As platinum conjugates with CA-4, compound **13** was expected to inhibit the formation of microtubules by interacting with the colchicines binding site of tubulin. To prove this, we investigated complex **13** that acts as an inhibitor of tubulin polymerization at dose-dependent manner in a tubulin polymerization assay. As shown in **Figure 5**, incubation with **13**, paclitaxel or CA-4 resulted in various degrees of inhibition of tubulin polymerization, depending on the property of each compound and the dose in the time dependency of this process. Among them, the positive drug paclitaxel (10 μM) was found to stimulate tubulin polymerization and CA-4 (10 μM) nearly completely inhibited tubulin polymerization as expected. For

compound **13**, an obvious inhibition of polymerization was observed at two concentrations, and the rate of assembly as well as the final amount of microtubules was lower than the control. However, cisplatin at 10 μM was barely effective in inhibition or stimulation of tubulin polymerization under the similar conditions compared with the control.

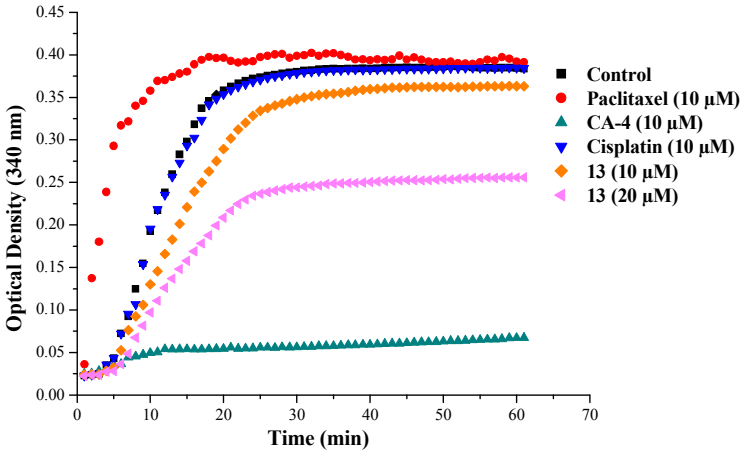

Figure 5. Effects of compound **13** on microtubule dynamics. Polymerization of tubulin at 37 °C in the presence of paclitaxel (10 μM), CA-4 (10 μM), cisplatin (10 μM) and **13** (10 μM and 20 μM) were monitored continuously by recording the absorbance at 340 nm over 60 min. The reaction was initiated by the addition of tubulin to a final concentration of 3.0 mg/mL.

Molecular Modeling. To elucidate the binding mode of platinum(IV) complexes, we performed a molecular docking postulated that they have the same binding site as colchicine and CA-4. The binding modes of these complexes in the colchicine binding site of tubulin are depicted in **Figure 6** and the Surflex docking scores obtained are

summarized in Table 4. The Surflex docking scores are 7.83 for CA-4, 11.29 for **13**, 10.37 for **15** and 10.68 for **14**, where higher scores indicate greater binding affinity. The order of the docking scores correlates with the IC_{50} values of the complexes for the growth inhibition of HepG-2 human liver cancer cells. Here we examine the docking details of complex **13** (whose IC_{50} values is 0.35 μM in HepG-2 cells) as compared with those of 3E22-colchicine, CA-4 and compound **9** (CA-4 derivative).

Table 4. Docking Scores (kcal/mol) for All Studied Compounds

Compd.	Total Score	Crash	polar	D_Score	PMF_Score	G-Score	Chem_Score	Cscore
13	11.29	-2.25	3.11	-235.69	-5.03	-392.55	-35.51	4
14	10.37	-2.28	4.91	-225.40	-9.48	-419.01	-42.66	5
15	10.68	-5.26	6.06	-262.27	-19.15	-440.78	-38.01	5
9	6.71	-0.98	1.79	-162.88	24.82	-221.82	-25.39	4
CA-4	7.83	-2.44	2.48	-137.09	10.98	-236.47	-23.67	4
3E22-ligand	6.70	-4.60	1.85	-158.29	18.38	-281.20	-26.83	4

Figure 6 A shows that the interacting mode of the cocrystallized 3E22-colchicine in the binding site, with 3,4,5-trimethoxy-phenyl rings placed in proximity to residue Cys241. In particular, 3E22-colchicine formed three hydrogen bonds with the polar amino acids Asn249, Ala 250 and Asn258, suggesting a probable stronger electrostatic interaction with the protein. In addition, the hydrophobic moiety of the 3E22-colchicine is well embedded in a pocket interacting with several hydrophobic residues making 3E22-colchicine bind tightly to tubulin. Not surprisingly, the accommodation of complex **13** in the binding site is similar to colchicine (**Figure 7**). Also in this case, docking simulations showed that the 3,4,5-trimethoxy-phenyl rings of complex **13** like colchicine can also be accommodated in the same hydrophobic groove, adopting an energetically

stable conformation. Moreover, the methoxy group in **13** as an acceptor establishes one hydrogen bond with Asn258, which is consistent with the observation that colchicine stabilizes the tubulin heterodimer and further confirms that this moiety is also crucial for binding. It is interesting to note that the crucial electrostatic interactions between the ammine of the Pt(IV) unit and residues Thr179, Ser178, Glu183 and Asn101 of the neighboring α-subunit were observed in the binding pocket, demonstrating a plausible competitive mechanism of action at the colchicine site.

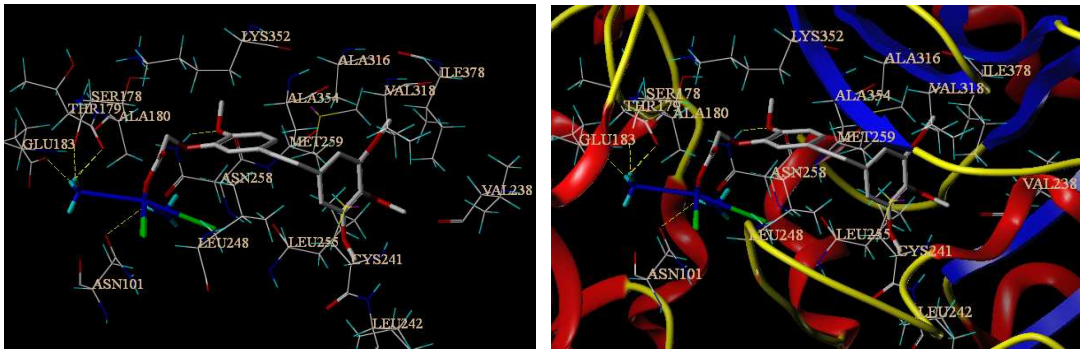

(A)

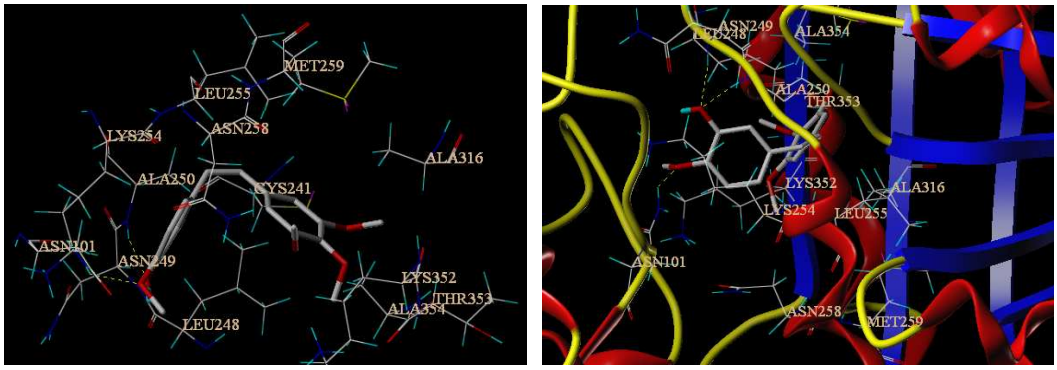

(B)

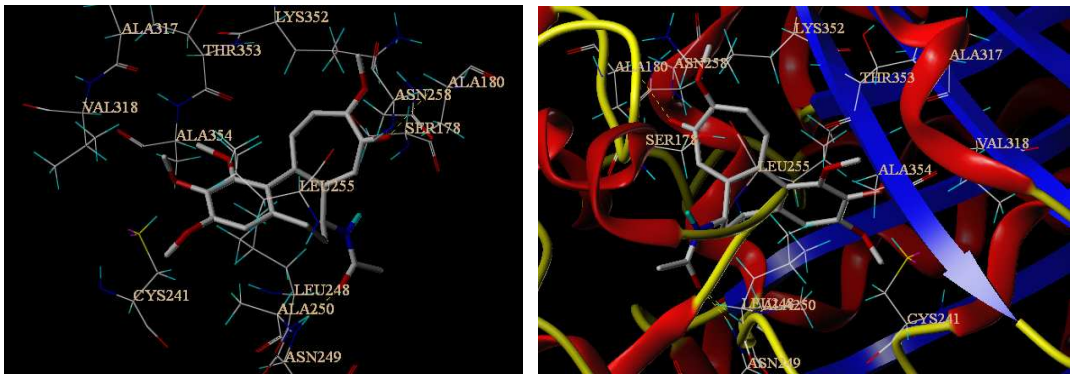

(C)

Figure 6. Molecular modeling of **CA-4**, 3E22-**colchicine** and **13** in complex with tubulin. Illustrated is the proposed binding mode and interaction between tubulin and selected compounds, (A) **13**, (B) **CA-4** and (C) 3E22-**colchicine**. The compounds and important amino acids in the binding pockets are shown in stick model, whereas tubulin is depicted in the ribbon model.

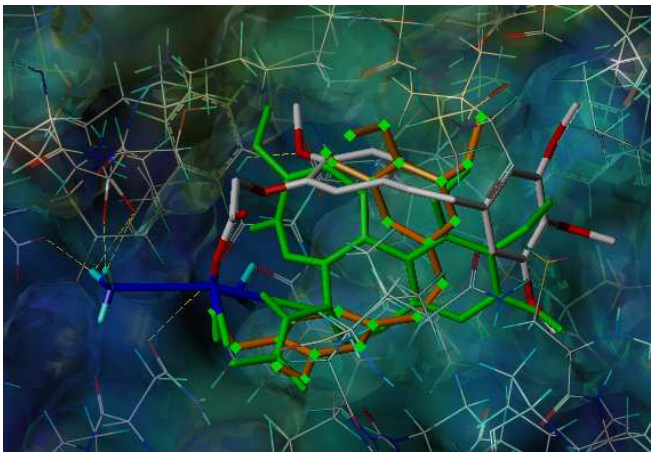

Figure 7. Comparison of the crystallographic structure of colchicines (in green), **CA-4** (in orange) in complex with tubulin (Protein Data Bank code 3E22) and the energetically most favorable pose of **13** (in gray) obtained by molecular docking simulation. Hydrogen atoms are omitted.

Competitive Binding to Colchicine Binding Site of Tubulin. To understand whether

the Pt(IV) conjugates can competitively bind to colchicine site of tubulin, we studied our representative compound to evaluate its effect on the binding of [^{3}H] colchicine to tubulin. The result is given in Table 5. For comparison, CA-4 was examined in contemporaneous experiments. In the colchicine binding studies, both compounds **9** and **13** are capable of inhibiting tubulin polymerization with calculated IC_{50} values of 7.56 μM and 7.91 μM, respectively. In addition, compound **13** showed the ability to compete with [^{3}H] colchicine in binding to tubulin. The binding potency of **13** (53.5%) to the tubulin colchicine binding site, comparable to compound **9** (55.8%), was much stronger than that of cisplatin but less than that of CA-4 (98%).

Table 5. Inhibition of Tubulin Polymerization and Colchicine Binding by Tested Compounds

Compounds (10 μM)	Tubilin assembly IC_{50} (μM)	Colchicines binding (% inhibition)
9	7.56±1.2	55.8±1.1
13	7.91±1.1	53.5±1.4
CDDP [a]	>100	1.2±0.3
CA-4	1.2±0.2	98.0±0.5

[a] Cisplatin

Effect on Cell Cycle Arrest. To investigate the effect of the synthetic Pt(IV) complexes on cell cycle arrest, we used flow cytometry to analyze the cell cycle distribution of HepG-2 cells following a 24 h treatment with complex **13** at different concentrations. Untreated cells were used as a negative control, and cells treated with cisplatin were used as a positive control. As shown in **Figure 8**, the most potent complex **13** was found to be as effective in arresting the cell cycle at G2/M phase as cisplatin.

With the untreated cells, the percentage of cells in the G0/G1 phase was at 73.34% with only 2.44% in the G2/M phase. After treatment with complex **13**, the percentage of cells in the G2/M phase increased to 18.09% (1 μM) and 63.30% (2 μM), respectively. These results compare favorably to 23.28% in the G2/M phase for cells treated with cisplatin (10 μM).

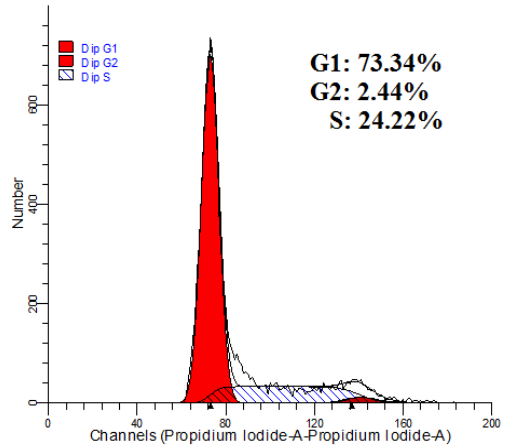

Control

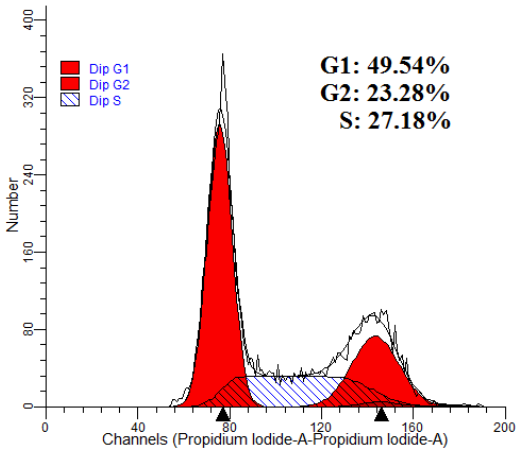

Cisplatin (10 μM)

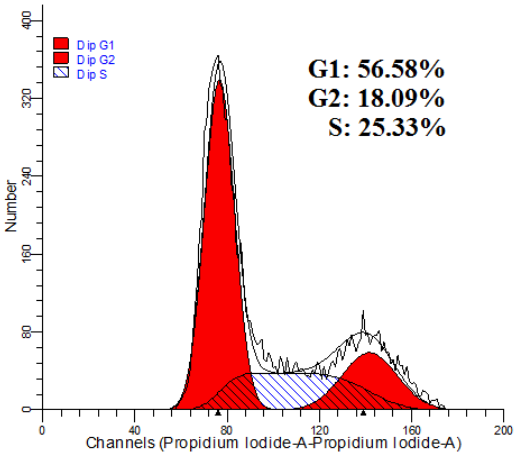

13 (1 μM)

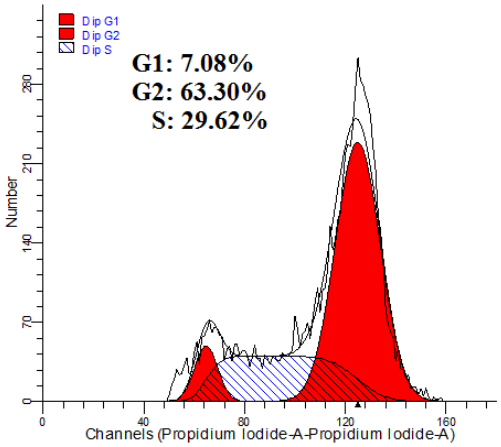

13 (2 μM)

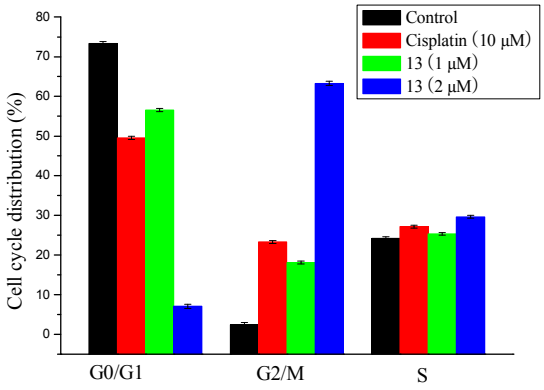

Figure 8. Effects of **13** on cell cycle phase arrest in HepG-2 cells. Cells were treated with 1 and 2 μM of **13** for 24 h. Then the cells were fixed and stained with PI to analyze DNA content by flow cytometry.

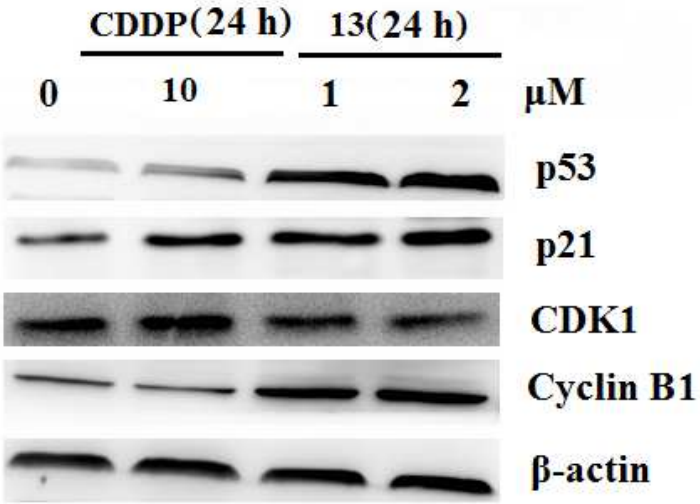

Figure 9. Western blot analysis of cyclin B1, CDK1, p21 and p53 after treatment of HepG-2 cells with **13** at the indicated concentrations and for the indicated times. β-actin antibody was used as reference control.

Furthermore, the molecular events involved in cellular response to the effective compound were investigated. The levels of regulatory proteins implicated in G2 arrest, including p21, CDK1, cyclin B1 and p53, were examined (**Figure 9**). Protein p21 plays a

significant role in G2 arrest through accumulation of inactive cyclin B1/p34^{cdc2} complex.[38-40] In fact, under the same conditions used for analysis of cell cycle perturbation (24 h exposure to 1, 2 μM for **13**), there was a noteworthy increase of p21 and p53 expression accompanied with up-regulation of cyclin B1, indicating an activation of the mitotic checkpoint following drug exposure. This effect was confirmed by the appearance of slower migrating forms of phosphatase CDK1 at 1 μM, followed by a strong reduction at 2 μM. Altogether these events are consistent with a pivotal role of p21 in G2 arrest as a consequence of inactivation of cyclin B1, and thus suggesting that the cells are effectively arrested at G2 phase of the cell cycle.

Complex 13 Induced Apoptotic Cell Death. In order to confirm whether the complex **13** induced reduction in cell viability was responsible for the induction of apoptosis, HepG-2 cells were co-stained with Annexin-V FITC and PI, and the number of apoptotic cells was estimated by flow cytometry. The tested complex was incubated with HepG-2 cells for 24 h at the increasing concentrations, and cisplatin served as a positive control. Q1−Q4 represent four different cell states: necrotic cells, late apoptotic or necrotic cells, living cells, and apoptotic cells, respectively (**Figure 10**). A dose-dependent increase in the percentage of apoptotic cells was noted after the cells were treated with complex **13** for 24 h at the concentrations of 2 μM and 4 μM. As shown in **Figure 10**, few (0.81%) apoptotic cells were present in the control panel, in contrast, the population rose to 23.58% at the concentration of 2 μM after treatment with **13** for 24 h. Further increase to 33.88% occurred after treatment with **13** at the concentration of 4 μM, while cisplatin

showed a lower population of apoptotic cells than complex **13**. Overall, the results clearly confirmed that complex **13** effectively induced apoptosis in HepG-2 cells.

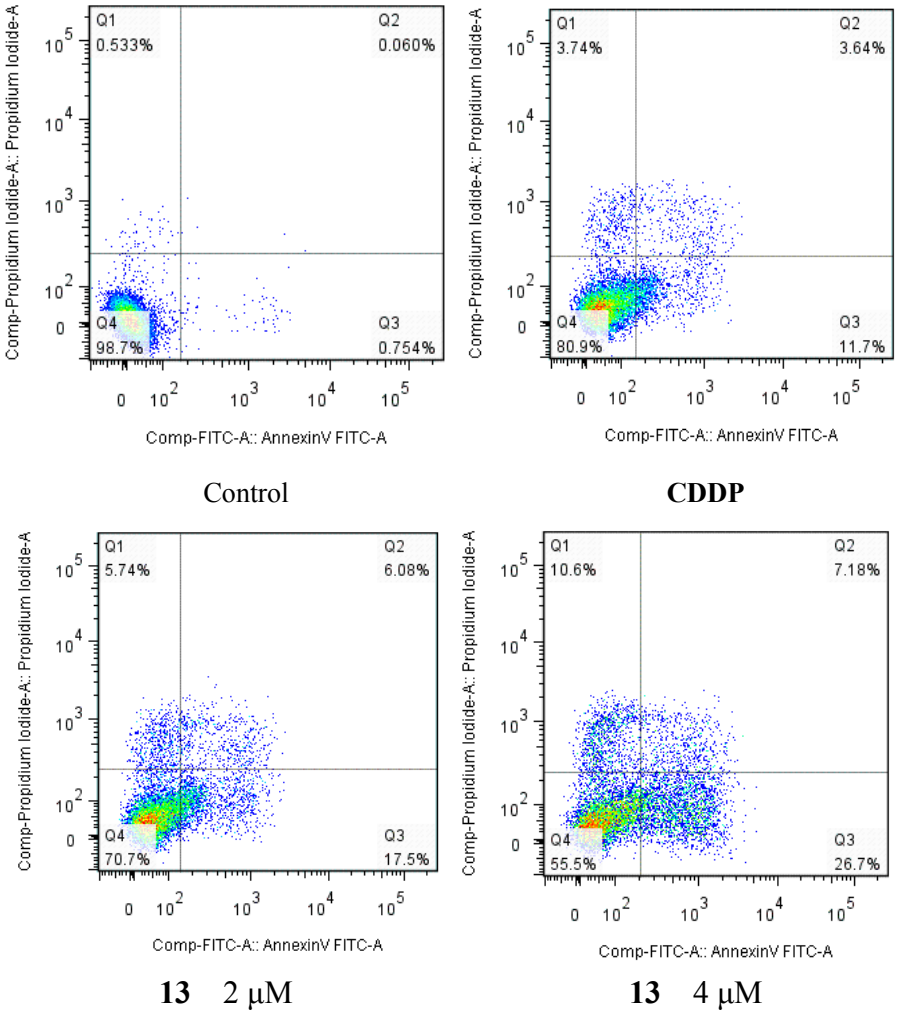

Figure 10. Representative flow cytometric histograms of apoptotic HepG-2 cells after 24 h treatment with **13**. The cells were harvested and labeled with annexin-V-FITC and PI, and analyzed by flow cytometry. Data are expressed as the mean ± SEM for five independent experiments.

Morphological Examination. The ability of complex **13** to induce apoptosis was further confirmed by analyzing the nuclear morphology of the exposed HepG-2 cells.

HepG-2 cells were treated with complex **13** for 24 h and stained with membrane-permeable blue Hoechst 33258 to detect apoptosis morphologically. As shown in **Figure 11**A, the Hoechst 33258 fluorescent photomicrographs of cultured HepG-2 cells treated with 2.0 and 4.0 μM complex **13** for 24 h, respectively, indicated that in the control cultures, the nuclei of HepG-2 cells appeared with regular contours and were round, whereas smaller nuclei and condensed chromatin were rarely seen. Treatment with 10.0 μM cisplatin or 2.0 μM complex **13** slightly changed the nuclear morphology (**Figure 11**B and 11C). It should be noted that the numbers of apoptotic nuclei containing condensed chromatin increased significantly as the result of treatment with 4.0 μM complex **13** (**Figure 11**D).

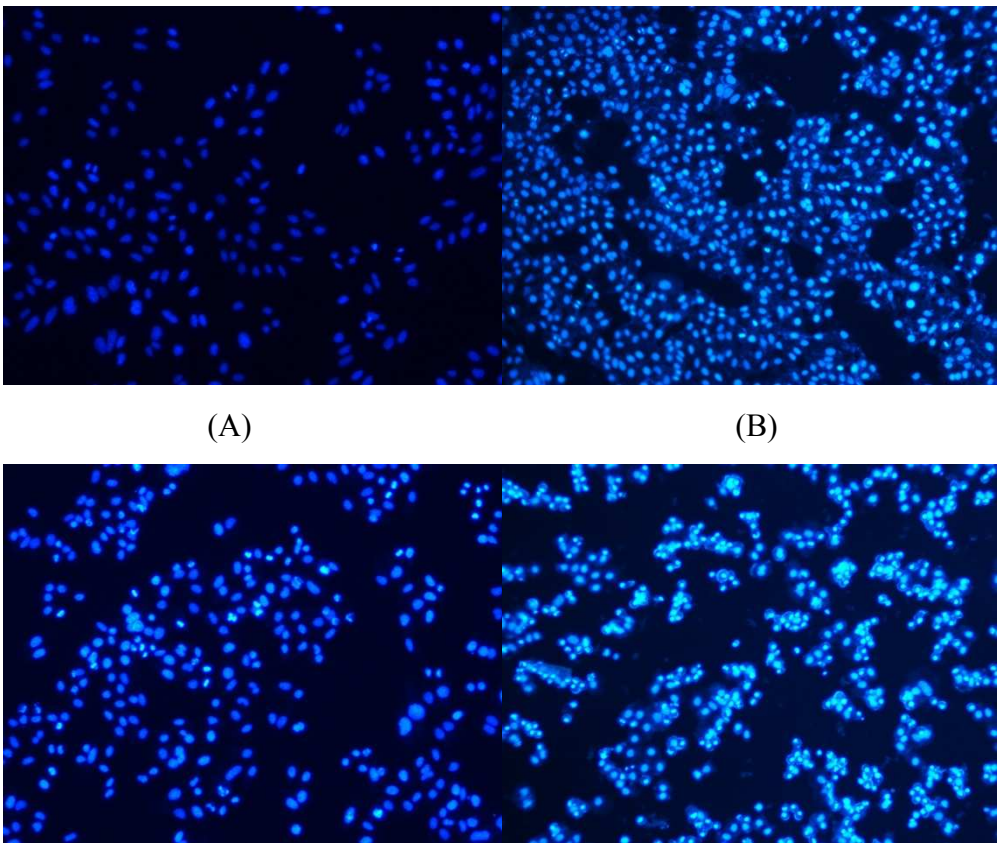

(A) (B)

(C) (D)

Figure 11. Morphological changes in the nuclei (typical of apoptosis) of cultured HepG-2 cancer cells. HepG-2 cancer cells treated with 2.0 and 4.0 μM **13** (C and D) and treated with 10.0 μM cisplatin for 24 h, respectively, and stained with Hoechst 33258. Selected fields illustrating occurrence of apoptosis were shown. Cells with condensed chromatin (brightly stained) were defined as apoptotic HepG-2 cancer cells. Images were acquired using a Nikon Te2000 deconvolution microscope (magnification 200×).

Complex 13 Triggered ROS Generation. Reactive oxygen species (ROS) are highly harmful elements to cells as they initiate oxidative stress and ultimately cause cellular damage. Excessive ROS generation renders cells vulnerable to apoptosis.[41-43] To determine whether **13** triggers ROS generation in HepG-2 cells to induce apoptosis, the ROS level was measured with and without (control) treatment of **13** (2.0, 4.0 and 6.0 μM) for 24 h, using the fluorescent probe 2,7-dichlorofluorescein diacetate (DCF-DA) by flow cytometry, and treatment of cisplatin (4.0 μM) as a positive control, respectively. As shown in **Figure 12**, the results indicated that complex **13** induced the production of significant amounts of ROS in HepG-2 cells. After exposure to 2.0 μM of complex **13** for 24 h, the ROS level was 33.6%, which is more than two times that of control and cisplatin. In all, these results proved that **13** causes oxidative imbalance in HepG-2 cells.

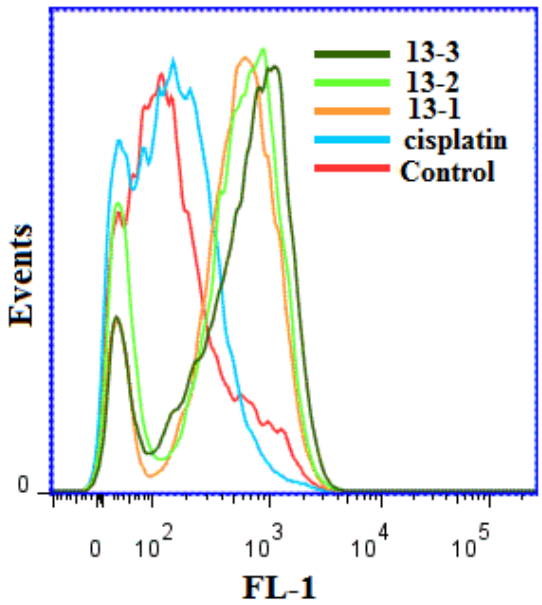

Figure 12. Assessment of the ROS production in HepG-2 cells. After 24 h incubations with **13**, cells were stained with DCF-DA and analyzed by flow cytometry. Data are expressed as the mean ± SEM of three independent experiments.

Effect of Complex 13 on Mitochondrial Depolarization. The loss of mitochondrial trans-membrane potential ($\Delta\psi_m$) is regarded as a limiting factor in the apoptotic pathway.[44,45] Therefore, the ability of mitochondria to maintain membrane potential after incubation with complex **13** was measured in HepG-2 cells using the fluorescent dyes JC-1. HepG-2 cells treated with complex **13** (2.0 and 4.0 μM) and cisplatin (4.0 μM), respectively, for 24 h, subsequently processed, which were stained with JC-1 dye and analyzed by flow cytometry. Complex **13** treated cells showed an increase in green/red fluorescence intensity indicating increased mitochondrial membrane depolarization compared with untreated cells (**Figure 13**). As shown in **Figure 13** B, the cisplatin induced dissipation of $\Delta\psi_m$ was significantly reduced in HepG-2 cells as compared with

13. The results revealed that the induction of apoptosis by complex **13** in HepG-2 cells is closely associated with mitochondrial function disruption. In fact, the dissipation of $\Delta\psi_m$ is characteristic of apoptosis and has been observed with platinum conjugates in different cell types.

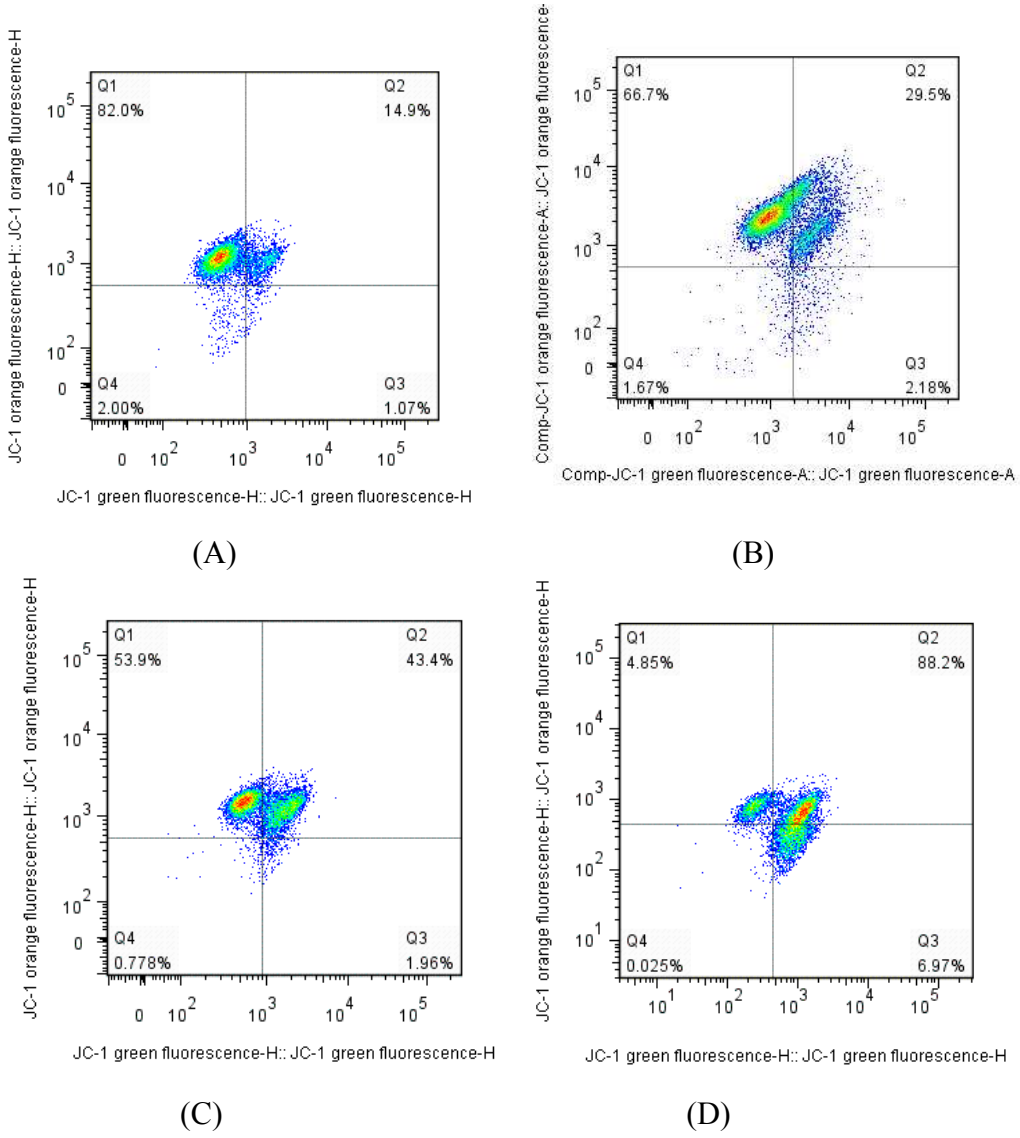

Figure 13. Assessment of mitochondrial membrane potential ($\Delta\psi_{mt}$) after treatment of HepG-2 cells with cisplatin (B) or compound **13** (C, D). Cells were treated with the indicated concentration of the compound for 24 h and then stained with the fluorescent

probe JC-1 and analyzed by flow cytometry. Data are presented as the mean ± SEM for three independent experiments.

Effect of Complex 13 Induced Apoptosis via an Intrinsic Apoptosis Pathway in HepG-2 Cells. The mitochondrial pathway is one of the major apoptosis pathways, which is often related to the loss of ΔΨm. The mitochondria-dependent apoptotic pathway is regulated by the Bcl-2 family of pro- and anti-apoptotic proteins, which induce the permeabilization of the mitochondrial outer membrane and cytochrome *c* released into the cytosol, resulting in the activation of the caspase cascade and the induction of apoptotic cell death.[46-49] To further understand the mechanism of action of the newly synthesized complex, the mitochondrial related apoptotic proteins of Bax, Bcl-2, cytochrome *c*, caspase-9, caspase-3 and PARP were tested in HepG-2 cells treated with complex **13** by the Western blot analysis. As shown in **Figure 14**, in comparison with the control cells, complex **13** induced a significant increase in the expression of Bax and a reduction in the levels of Bcl-2, in a time dependent fashion. The result indicated that treatment with **13** could shift the ratio of Bax/ Bcl-2 proteins and thus lead to collapse of the mitochondrial membrane potential. Moreover, after HepG-2 cells were treated with 5.0, and 10.0 μM **13** for 24 h, the release of cytochrosome *c* increased in a concentration-corresponding manner. Subsequently, the activation of downstream caspases, including caspase-3 and caspase-9, was observed, all of which could trigger apoptosis of tumor cells. Exposure of HepG-2 cells to this complex caused a dramatic increase in the levels of caspase-9, caspase-3 and cleaved-PARP, as compared with

control cells. These observations suggested that complex **13** might induce HepG-2 cells apoptosis through a mitochondrial mediated pathway and caspase cascade.

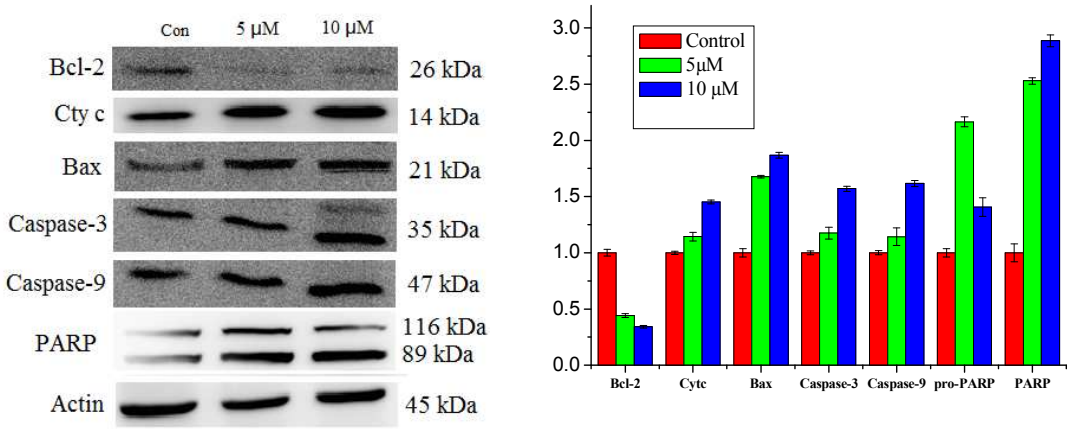

Figure 14. Western blot analysis of Cyt *c*, Bax, Bcl-2, PARP，caspase-9 and caspase-3 after treatment of HepG-2 cells with **13** at the indicated concentrations and for the indicated times. β-actin antibody was used as reference control.

Anti-tumor Effect of Complex 13 in Vivo. To validate the efficacy of complex **13** to inhibit tumor growth in vivo, the nude mouse HepG-2 tumor xenograft models were established by subcutaneously injecting HepG-2 cells in the logarithmic phase into the right armpit of the mice. When the model was well-established, mice with tumors at the volume of 100−150 mm^3 were randomly divided into six groups: (1) cisplatin (5 mg/kg) treated group; (2) CA-4 (5 mg/kg) treated group; (3) cisplatin (5 mg/kg) + CA-4 (5 mg/kg) treated group; (4) complex **13** (5 mg/kg) treated group; (5) complex **13** (10 mg/kg) treated group; (6) vehicle treated group (5% dextrose injection). The mice were administered intravenously with the above-mentioned formulations once every seven days for 21 days. As shown in **Figure 15**, the growth of HepG-2 tumor xenograft was

significantly suppressed by 51.2% and 59.4% (percent of inhibition rate [IR] values) after iv administration of complex **13** at 5 and 10 mg/kg compared with vehicle control group, respectively. It was found that complex **13** presented better antitumor activity than CA-4 (IR, 39.6%) in vivo, as the similar results were also observed in the tumor weight and volume change (**Figures** 15 C and D). It was noted that complex **13** displayed better anticancer activity in vitro, but showed a little lower value of IR in vivo than either cisplatin (IR, 66.0%) or cisplatin+CA-4 (IR, 71.7%), respectively. Despite the cisplatin treatment also significantly caused tumor growth inhibition, its toxicity was apparent, as evidenced by loss of body weight compared with **13**. In all, complex **13** exhibited high antitumor activity and low toxicity both in vitro and in vivo, suggesting that it could be used as a drug candidate for further research on the therapy of hepatic carcinoma.

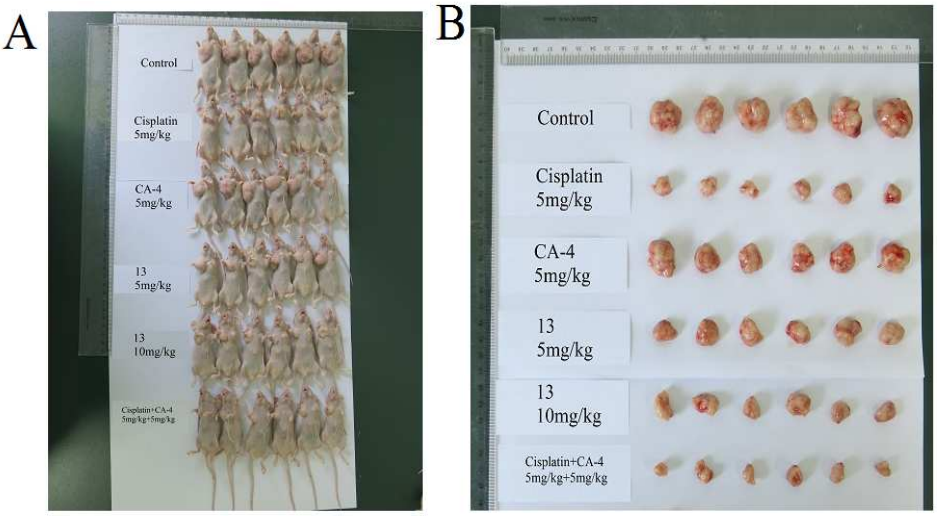

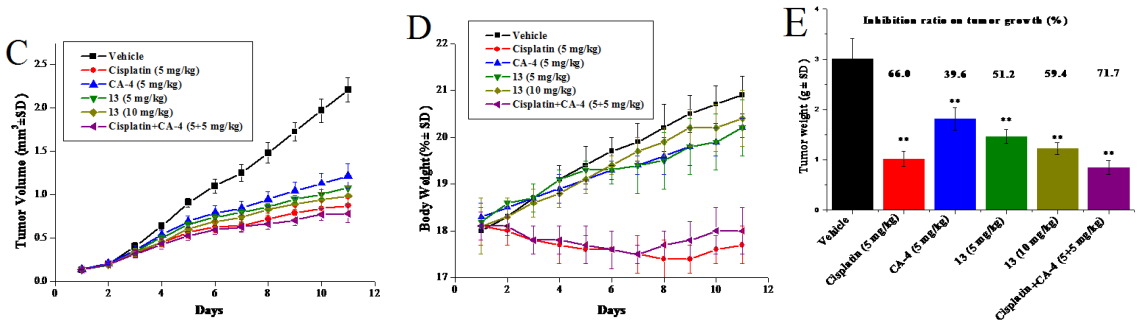

Figure 15. In vivo anti-tumor activity of complex **13** in mice bearing HepG-2 xenograft. (A-B) After administered with complex **13** at the dose of 5 and 10 mg/kg, cisplatin at the dose of 5 mg/kg, CA-4 at the dose of 5 mg/kg, cisplatin+CA-4 (cisplatin: dosage of 5 mg/kg, CA-4: dosage of 5 mg/kg) for 21 days, the mice were sacrificed and weighed the tumors. (C) The tumor volume of the mice in each group during the observation period. (D) The weight of the excised tumors of each group. (E) The body weight of the mice from each group at the end of the observation period. The data were presented as the mean ± SEM. *P < 0.05.

CONCLUSION

In summary, conjugation of the CA-4 derivative (**9**) to the Pt(IV) units derived cisplatin, oxaliplatin and DACHPt, respectively, has resulted in three Pt(IV) complexes containing the moiety of a tubulin inhibitor. Each Pt(IV) compound showed higher cytotoxicity than its Pt(II) counterpart against all the tested cancer cell lines including cisplatin resistant ones, but exhibited less toxic than all the corresponding Pt(II) complexes against normal human liver cell LO2. Additional molecular docking studies revealed that the CA-4 moiety carried a Pt(IV) unit to the binding of colchicine to tubulin, in which the ammine group of the Pt(IV) unit established the crucial electrostatic interactions with the

neighboring α-subunit. Further mechanistic studies on complex **13** indicated that it can effectively enter cells, arrest the cell cycle at G2/M phases, heavily inhibit the assembly of tubulin, and dramatically increase the apoptosis level. Our investigation also revealed that the induction of apoptosis by **13** was associated with down-regulation of Bcl-2, dissipation of the mitochondrial trans-membrane potential, and activation of caspase-3, which are coupled with terminal events of apoptosis, such as PARP cleavage. These results indicated that complex **13** has a distinct mechanism of action to kill cancer cells. Although CA-4 might have other targets except tubulin, it indeed promotes the anticancer activity of cisplatin by inhibiting the assembly of tubulin. Remarkably, complex **13** exhibited much effective inhibition on tumor growth in the HepG-2 xenograft mouse model with high safety in vivo. Although we cannot exclude the possibility that the promoted cellular uptake of platinum, due to the hydrophobic feature of the CA-4 moiety in complex **13**, may also contribute the elevated apoptosis and cytotoxicity to one specific cellular event in HepG-2 cells, the unique property of a single prodrug on cell cycle arrest together with the tubulin inhibition clearly indicated that the CA-4 moiety plays a key role in the cytotoxicity of complex **13**, not only by facilitating the cell entrance. Nevertheless, this study highlights the advantage of the "dual action" complexes conjugating cisplatin with a tubulin inhibitor, in which the resulting single "multi-action" Pt(IV) prodrug can trigger many different events that lead to the death of the cancer cells.

EXPERIMENTAL SECTION

Materials and Instruments. All chemicals and solvents were of analytical reagent

grade and used without further purification, unless noted specifically. The purity of all target compounds were used in the biophysical and biological studies was ≥95%. The Acitn, Bax, Bcl-2, cytochrome c, caspase-9, caspase-3, PARP, cyclin B, CDK1, p21 and p53 antibodies were purchased from Imgenex, USA. All tumor cell lines were obtained from Nanjing KeyGEN BioTECH company (China). ^{1}H NMR and ^{13}C NMR spectra were recorded in $CDCl_3$ or d_6-DMSO with a Bruker 300 or 400 MHz spectrometer. Elemental analyses of C, H, and N used a Vario MICRO CHNOS elemental analyzer (Elementary). Mass spectra were measured on an Agilent 6224 TOF LC/MS instrument.

Synthesis of Compound 2. To a solution of compound **1** (5.0 g, 25.5 mmol) in dry MeOH (50 mL), $NaBH_4$ (2.9 g, 76.5 mmol) was added at 0 °C, then the mixture was stirred at room temperature for 2 h and monitored by TLC. After completion of reaction, the reaction was quenched with ice water, and the solvent was removed under the reduced pressure. The residue was added water (100 mL), then was extracted with CH_2Cl_2. The combined organic layer was washed with saturated NaCl solution, dried over anhydrous Na_2SO_4 and concentrated under reduced pressure to give the desired product (4.9 g, yield 97.0%) as a white oil. The crude product, used directly without further purification, was characterized by ^{1}H-NMR spectrum. ^{1}H NMR (300 MHz, $CDCl_3$): δ 6.58 (s, 2H), 4.61 (s, 2H), 3.84 (d, J = 7.7 Hz, 9H, 3×-OCH_3), 1.89 (s, 1H).

Synthesis of compound 3. To a solution of compound **2** (4.9 g, 24.7 mmol) in dry DCM (35 mL), PBr_3 (2.9 g, 76.5 mmol) in DCM (15 mL) was dropwise added at 0 °C,

then the mixture was stirred at room temperature for 30 mins. After completion of reaction, the reaction was quenched with ice water and extracted with CH_2Cl_2. The combined organic layer was washed with saturated NaCl solution, dried over anhydrous Na_2SO_4 and concentrated under reduced pressure. The residue was purified on a silica gel column to give the desired product (5.5 g, yield 85.9%) as a white solid. ^{1}H NMR (300 MHz, $CDCl_3$): δ 6.62 (s, 2H), 4.46 (s, 2H), 3.85 (d, J = 7.6 Hz, 9H).

Synthesis of Compound 4. To a solution of compound **3** (4.9 g, 18.8 mmol) in dry toluene (100 mL), PPh_3 (6.4 g, 24.5 mmol) was added in portions and stirred at reflux for 3 h. After completion of reaction, the reaction mixture was cooled at room temperature and removed the solvent under the reduced pressure, the white solid was washed with toluene. The solid was dried over in vacuum to give the desired product (8.5 g, yield 86.7%) as a white solid. The crude product, used directly without further purification, was characterized by ^{1}H-NMR spectrum. ^{1}H NMR (300 MHz, DMSO-*d6*): δ 7.94 – 7.89 (m, 3H), 7.81 – 7.72 (m, 6H), 7.71 (s, 2H), 7.69 – 7.64 (m, 4H), 6.24 (d, J = 2.4 Hz, 2H), 5.03 (d, J = 15.2 Hz, 2H), 3.62 (s, 3H), 3.41 (s, 6H).

Synthesis of Compound 5. To a solution of 3-hydroxy-4-methoxybenzaldehyde (3.5 g, 23.0 mmol) and Et_3N (4.6 g, 46.0 mmol) in DMF (30 mL), TBDMSCl (5.2 g, 34.5 mmol) was added at 0 °C, then the mixture was stirred at room temperature for 2 h. After completion, the reaction mixture was poured into ice water (500 mL) and extracted with CH_2Cl_2 (2×150 mL). The combined organic layer was washed with saturated NaCl

solution (three times), dried over anhydrous Na_2SO_4 and concentrated under reduced pressure to give yellow oil (5.8 g, yield 95.1%) which was used directly without further purification. ^{1}H NMR (300 MHz, $CDCl_3$): δ 9.82 (s, 1H), 7.47 (dd, J = 8.3, 1.9 Hz, 1H), 7.37 (d, *J* = 1.9 Hz, 1H), 6.95 (d, *J* = 8.3 Hz, 1H), 3.90 (s, 3H), 1.01 (s, 9H), 0.17 (d, J = 0.9 Hz, 6H); HR-MS (m/z) (ESI): calcd for $C_{14}H_{22}O_3Si$ [M+H$^+$]: 267.14165, found: 267.14303.

Synthesis of 6a and 6b. To a solution of compound **4** (5.8 g, 11.1 mmol) in dry DCM (50 mL), NaH (2.2 g, 55.5 mmol) was added at 0 °C. After the mixture was stirred at the same temperature for 0.5 h, compound **5** (2.9 g, 11.1 mmol) in dry DCM (10 mL) was added dropwise. The reaction was stirred at room temperature for overnight, then the reaction mixture was quenched with ice water, washed with water. The organic phase was washed with saturated NaCl solution, dried over anhydrous Na_2SO_4 and concentrated under vacuum. The residue was purified on a silica gel column eluted with petroleum ether/ethyl acetate (19:1= V:V) to give the desired product **6a** (2.1 g, yield 44.0%) as a yellow oil and **6b** (2.5 g, yield 52.4%) as a white solid. **6a**: ^{1}H NMR (300 MHz, $CDCl_3$): δ 6.85 (dd, *J* = 8.2, 1.7 Hz, 1H), 6.79 (d, *J* = 1.9 Hz, 1H), 6.73 (d, *J* = 8.3 Hz, 1H), 6.50 (s, 2H), 6.43 (t, *J* = 8.5 Hz, 2H), 3.83 (s, 3H), 3.78 (s, 3H), 3.70 (s, 6H), 0.93 (s, 9H), 0.06 (s, 6H); HR-MS (m/z) (ESI): calcd for $C_{24}H_{34}O_5Si$ [M+Na]: 453.20732, found: 453.20235. **6b**: ^{1}H NMR (300 MHz, $CDCl_3$): δ 7.05 (d, *J* = 8.4 Hz, 2H), 6.88 – 6.82 (m, 3H), 6.71 (s, 2H), 3.92 (s, 6H), 3.87 (s, 3H), 3.83 (s, 3H), 1.03 (s, 9H), 0.19 (s, 6H); HR-MS (m/z)

(ESI): calcd for $C_{24}H_{34}O_5Si$ [2M+Na]: 883.42847, found: 883.35081.

Synthesis of Compound 7(CA-4). To a solution of compound **6a** (2.7 g, 6.28 mmol) in dry MeOH (30 mL), 1N MeOH/HCl (10 mL) was added. The reaction mixture was stirred at 50 °C for 2 h, and then cooled to the room temperature. After the solvent was removed by evaporation, the resulting residue was diluted with water (100 mL) and extracted with CH_2Cl_2 (2×100 mL). The organic phase was dried over anhydrous Na_2SO_4 and concentrated under vacuum. The residue was purified on a silica gel column eluted with petroleum ether/ethyl acetate (3:1= V:V) to give the desired product (1.8 g, yield 94.7%) as a white solid. ^{1}H NMR (300 MHz, $CDCl_3$): δ 6.92 (d, *J* = 1.7 Hz, 1H), 6.79 (dd, *J* = 8.3, 1.7 Hz, 1H), 6.73 (d, *J* = 8.4 Hz, 1H), 6.52 (s, 2H), 6.47 (d, *J* = 12.2 Hz, 1H), 6.40 (d, *J* = 12.2 Hz, 1H), 5.53 (s, 1H), 3.86 (s, 3H), 3.84 (s, 3H), 3.70 (s, 6H); HR-MS (m/z) (ESI): calcd for $C_{18}H_{20}O_5$ [M+H]: 317.13890, found: 317.13805.

Synthesis of Compound 8. To a solution of compound **7** (1.6 g, 5.06 mmol) in DMF (25 mL), α-bromoethyl acetate (1.1 g, 6.58 mmol), K_2CO_3 (1.4 g, 10.1 mmol) and KI (84 mg, 0.51 mmol) were added. The mixture was stirred at room temperature for overnight, the reaction was monitored by TLC. After completion of reaction, the mixture was diluted with water (300 mL) and extracted with CH_2Cl_2 (2×150 mL). The organic phase was dried over anhydrous Na_2SO_4 and concentrated under reduced pressure. The residue was purified on silica gel column eluted with petroleum ether/ethyl acetate (3:1= V:V) to give the desired product (1.6 g, yield 80.0%) as a yellow oil. ^{1}H NMR (400 MHz, $CDCl_3$): δ

6.91 (dd, J = 8.3, 1.9 Hz, 1H), 6.79 (d, J = 8.3 Hz, 1H), 6.74 (d, J = 1.9 Hz, 1H), 6.50 – 6.45 (m, 3H), 6.43 (d, J = 12.1 Hz, 1H), 4.49 (s, 2H), 4.19 (q, J = 7.1 Hz, 2H), 3.86 (s, 3H), 3.83 (s, 3H), 3.69 (s, 6H), 1.24 (t, J = 7.1 Hz, 3H); HR-MS (m/z) (ESI): calcd for $C_{22}H_{26}O_7$ [M+H]: 403.17568, found: 403.17739.

Synthesis of Compound 9. To a solution of compound **8** (1.5 g, 3.73 mmol) in THF (30 mL) lithium hydroxide (470 mg, 11.2 mmol) was added and stirred at room temperature for 2 h. The reaction mixture was adjusted pH = 2 with 2 N HCl solution, the mixture was added water (100 mL) and extracted with CH_2Cl_2 (2×100 mL), then the organic phase was dried over anhydrous Na_2SO_4 and concentrated under reduced pressure to give the desired product (1.2 g, yield 85.7%) as a white solid. ^{1}H NMR (300 MHz, $CDCl_3$): δ 6.94 (d, J = 7.9 Hz, 1H), 6.80 (d, J = 8.2 Hz, 2H), 6.46 (d, J = 4.9 Hz, 4H), 4.51 (s, 2H), 3.86 (s, 3H), 3.83 (s, 3H), 3.69 (s, 6H); HR-MS (m/z) (ESI): calcd for $C_{20}H_{22}O_7$ [M+H]:375.14438, found: 375.14217.

General Syntheses of Compounds 10-12 According to the Reported Procedure.[36] To a solution of cisplatin, dichloro(trans-1,2-diaminocyclohexane)platinum or oxaliplatin (8.0 mmol) in water (450 mL), NCS (1.2 g, 8.8 mmol) in 450 mL of water was added dropwise. After the mixture was stirred at room temperature for overnight, the black deposit was removed by filtration. The filtrate was concentrated under reduced pressure and yellow solid precipitated. The solid was collected and washed with ethanol and ether, respectively, then dried in vacuum to give the desired product. This crude product was

used directly without further purification.

*Compound **10***. Yield: 92.1%. ^{1}H NMR (300 MHz, DMSO-*d6*): δ 6.15 – 5.22 (m, 6H).

*Compound **11.*** Yield: 92.5%. ^{1}H NMR (300 MHz, DMSO-*d6*): δ 7.51 – 7.20 (m, 2H), 7.09 – 6.56 (m, 2H), 2.83 – 2.56 (m, 2H), 2.05 (t, *J* = 9.1 Hz, 2H), 1.59 – 1.37 (m, 4H), 1.16 – 0.90 (m, 2H).

*Compound **12***. Yield: 89.3%. ^{1}H NMR (300 MHz, DMSO-*d6*): δ 8.01 – 7.57 (m, 2H), 7.31 – 6.83 (m, 2H), 2.62 – 2.54 (m, 2H), 1.99 (d, *J* = 15.0 Hz, 2H), 1.64 – 1.34 (m, 4H), 1.11 – 0.99 (m, 2H).

General Syntheses of Compounds 13-15. To a solution of compound **9** (140 mg, 0.374 mmol), TBTU (164 mg, 0.510 mmol) and Et_3N (52 mg, 0.510 mmol) in dry DMF (4 mL), compound **10, 11 or 12** (0.340 mmol) was added in portions. The mixture was stirred at room temperature for overnight. After completion of reaction, the whole mixture was added CH_2Cl_2 (120 mL), then extracted two times with water (100 mL). The organic phase was dried over anhydrous Na_2SO_4 and concentrated under reduced pressure. The residue was purified on silica gel column eluted DCM/ MeOH (50:1) to give the desired product as a yellow solid.

*Compound **13***. Yield: 53.0%. ^{1}H NMR (300 MHz, DMSO-*d6*): δ 6.87 (d, *J* = 7.2 Hz, 3H), 6.55 (s, 2H), 6.50 (d, *J* = 12.4 Hz, 1H), 6.43 (d, *J* = 12.4 Hz, 1H), 6.21 (s, 6H), 4.49

(s, 2H), 3.73 (s, 3H), 3.64 (s, 3H), 3.60 (s, 6H); ^{13}C NMR (75 MHz, DMSO-*d6*): δ 175.96, 152.99, 148.68, 147.75, 137.18, 132.79, 129.97, 129.85, 129.06, 121.85, 115.63, 112.45, 106.52, 66.68, 60.64, 56.13, 46.21; HR-MS (m/z) (ESI): calcd for $C_{20}H_{27}Cl_3N_2O_7Pt$ [M-H$^+$]:707.05316, found: 707.04872. Elem Anal. Calcd (%) for $C_{20}H_{27}Cl_3N_2O_7Pt$: C, 33.89; H, 3.84; N, 3.95; found: C, 33.71; H, 3.99; N, 3.67.

*Compound **14***. Yield: 69.3%. ^{1}H NMR (400 MHz, DMSO-*d6*): δ 9.08 (t, *J* = 9.7 Hz, 1H), 8.16 (s, 1H), 7.90 (s, 1H), 7.67 – 7.44 (m, 1H), 6.91 – 6.82 (m, 2H), 6.75 (s, 1H), 6.53 (s, 2H), 6.50 (d, *J* = 12.2 Hz, 1H), 6.42 (d, *J* = 12.2 Hz, 1H), 4.58 (s, 2H), 3.74 (s, 3H), 3.64 (s, 3H), 3.60 (s, 6H), 2.15 – 2.02 (m, 2H), 1.57 – 1.18 (m, 4H), 1.11 – 0.85 (m, 4H); ^{13}C NMR (100 MHz, DMSO-*d6*): δ 178.12, 152.99, 148.52, 147.63, 137.29, 132.75, 129.95, 129.79 129.31, 121.61, 114.80, 112.60, 106.65, 65.34, 63.99, 62.83, 60.56, 56.14, 56.17, 31.39, 3136, 24.06, 23.95; HR-MS (m/z) (ESI): calcd for $C_{26}H_{35}Cl_3N_2O_7Pt$ [M+H$^+$]: 788.12358, found: 789.11737. Elem Anal. Calcd (%) for $C_{26}H_{35}Cl_3N_2O_7Pt$: C, 39.58; H, 4.47; N, 3.55; found: C, 39.64; H, 4.53; N, 3.28.

*Compound **15***. Yield: 56.5%. ^{1}H NMR (400 MHz, DMSO-*d6*): δ 8.50 – 8.24 (m, 2H), 8.07 (t, *J* = 9.4 Hz, 1H), 7.67 (t, *J* = 10.2 Hz, 1H), 6.89 – 6.83 (m, 2H), 6.73 (d, *J* = 1.2 Hz, 1H), 6.54 (s, 2H), 6.50 (d, *J* = 12.2 Hz, 1H), 6.43 (d, *J* = 12.2 Hz, 1H), 4.57 (s, 2H), 3.73 (s, 3H), 3.64 (s, 3H), 3.60 (s, 6H), 2.09 – 1.99 (m, 2H), 1.61 – 0.99 (m, 8H); ^{13}C NMR (100 MHz, DMSO-*d6*): δ 175.54, 163.60, 152.98, 148.60, 147.51, 137.19, 132.74, 129.85, 129.79, 129.25, 121.84, 114.68, 112.60, 106.51, 99.99, 66.49, 62.08,

61.64, 60.53, 56.12, 56.09, 31.33, 31.02, 23.97, 23.94; HR-MS (m/z) (ESI): calcd for $C_{28}H_{35}ClN_2O_{11}Pt$ [M+Na]: 829.11477, found: 829.10064. Elem Anal. Calcd (%) for $C_{28}H_{35}ClN_2O_{11}Pt$: C, 41.72; H, 4.38; N, 3.48; found: C, 41.66; H, 4.25; N, 3.23.

The released ability of Pt(IV) complexes under reduction with ascorbic acid. The released ability of Pt(IV) complexes in a solvent comprised of acetonitrile/water (60:40, v:v) was studied by HPLC. The standard compounds were made by adding ascorbic acid, compound **9** and Pt(IV) complexes, separately, to a solvent containing 60.0% acetonitrile and 40.0% water. The incubation was generated by adding test compounds to a solvent containing 60% acetonitrile and 40% water, which was performed at 25 °C for 0 h, 1 h and 2 h, separately. Reversed-phase HPLC was carried out on a 250×4.5 mm ODS column. HPLC profiles were recorded on UV detection at 210 nm. Mobile phase consisted of acetonitrile /Water (60:40, v/v), and flow rate was 1.0 mL/min. The samples were taken for HPLC analysis after filtered by 0.45 μm filter.

Cell Culture. All adherent cell lines including human colorectal carcinoma cell line (HCT-116), hepatocellular carcinoma cell line (HepG-2), non-small cell lung cancer cell line (A549), gastric cancer cell line (SGC7901), cisplatin-resistant gastric cancer cell line (SGC7901/CDDP), breast cancer cell line (MCF-7), large cell lung cancer cell line (NCI-H460), cisplatin-resistant non-small cell lung cancer cell line (A549/CDDP), hepatocellular carcinoma cell line (Bel-7404) and human liver cell line (LO2), were cultured in a humidified, 5% CO_2 atmosphere at 37°C, and maintained in monolayer

culture in DMEM medium supplemented with 10% fetal bovine serum (FBS), 100 mg/mL of streptomycin and 100 mg/mL of penicillin.

Cytotoxicity Analysis. A549, Bel-7404, HCT-116, HepG-2, MCF-7, NCI-H460, SGC-7901,7901/CDDP, A549/CDDP and LO2 cell lines were grown on 96-well plates at a cell density of 1×10^5 cells/well in DMEM medium with 10% FBS. The plates were incubated at 37 ℃ in a humidified atmosphere of 5% CO_2/95% air for overnight. Therewith, the cells were exposed to different concentrations of selected compounds, cisplatin and CA-4, and incubated for another 72 h. The cells were stained with 10 μL of MTT at incubator for about 4 h. The medium was thrown away and replaced by 100 mL DMSO. The O.D. Value was read at 570/630 nm enzyme labeling instrument.

Cellular Uptake Test. HepG-2 cells were seeded in 6-well plates. After the cells reached about 80% confluence, 20 μM of cisplatin, **13** or **14** was added, respectively**.** After 12 h incubation, cells were collected and washed three times with ice-cold PBS, then centrifuged at 1000×g for 10 min and resuspended in 1 mL PBS. A volume of 100 μL was taken out to determine the cell density. The rest of the cells was spun down and digested at 65 ^{o}C in 200 μL 65% HNO_3 for 10 h. The Pt level in cells was measured by ICP-MS.

Tubulin Polymerization Assay in Vitro and Competitive Inhibition Assays. Tubulin polymerization assay was monitored by the change in optical density at 340 nm using a modification of methods described by Jordan et al.[50] Purified brain tubulin polymerization kit was purchased from Cytoskeleton (BK006P, Denver, CO). The final buffer concentrations for tubulin polymerization contained 80.0 mM

piperazine-N,N′-bis(2-ethanesulfonic acid) sequisodium salt (pH 6.9), 2.0 mM $MgCl_2$, 0.5 mM ethylene glycol bis(β-aminoethyl ether)-N,N,N′,N′-tetraacetic acid (EGTA), 1 mM GTP, and 10.2% glycerol. Test compounds were added in different concentrations, and then all components except the purified tubulin were warmed to 37 °C. The reaction was initiated by the addition of tubulin to a final concentration of 3.0 mg/mL. Paclitaxel and CA-4 were used as positive controls under similar experimental conditions. The optical density was measured for 1 h at 1 min intervals in BioTek's Synergy 4 multifunction microplate spectrophotometer with a temperature controlled cuvette holder. Assays were performed according to the manufacturer's instructions and under conditions similar to those employed for the tubulin polymerization assays described above.[51,52]

Competitive Inhibition Assays. The competitive binding activity of inhibitors was evaluated using a [^{3}H]colchicine competition scintillation proximity (SPA) assay.[53] In brief, 0.08 μM [^{3}H]colchicine was mixed with the test compound and biotinylated porcine tubulin (1.3 mg/ml) in the incubation buffer (80 mM PIPES, pH 6.9, 2.0 mM $MgCl_2$, 0.5 mM EGTA, 10% glycerol, 1 mM GTP) at 37 °C for 2 h. Varying concentrations (5, 10, 15, 20, and 40 μM) of the test compounds were used to compete with colchicine originally bound to tubulin. After incubation, the filtrate was obtained as described previously.[54] The ability of the test compounds to inhibit colchicine binding to tubulin was measured as described [55] except that the reaction mixtures contained 1 μM tubulin, 5 μM [^{3}H]colchicine, and 5 μM test compound.

Molecular Modeling. All the docking studies were carried out using Sybyl-X 2.0 on a windows workstation. The initial coordinates for tubulin was taken from the crystal structure of tubulin in complex with colchicine (PDB: 3E22.pdb).[56,57] The synthetic

analogues, including the parent compound CA-4, were selected for the docking studies. The 3D structures of these selected compounds were first built using Sybyl-X 2.0 sketch followed by energy minimization using the MMFF94 force field and Gasteiger−Marsili charges. We employed Powell's method for optimizing the geometry with a distance dependent dielectric constant and a termination energy gradient of 0.05 kcal/mol. All the selected compounds were automatically docked into the binding pocket of tubulin by an empirical scoring function and a patented search engine in the Surflex docking program. Before the docking process, the natural ligand was extracted; the water molecules were removed from the crystal structure. Subsequently, the protein was prepared by using the Biopolymer module implemented in Sybyl. The polar hydrogen atoms were added. The automated docking manner was applied in the present work. Other parameters were established by default in the software. Surflex-Dock total scores, which were expressed in $-\log_{10}$ (K_d) units to represent binding affinities, were applied to estimate the ligand-receptor interactions of newly designed molecules.

Cell Cycle Analysis. HepG-2 cells line were treated with different concentrations of compound **13**. After 24 h of incubation, cells were washed twice with ice-cold PBS, fixed and permeabilized with ice-cold 70% ethanol at -20 ℃ overnight. The cells were treated with 100 μg /mL RNase A at 37 ℃ for 30 min after washed with ice-cold PBS, and finally stained with 1 mg/ml propidium iodide (PI) in the dark at 4 ℃ for 30 min. Analysis was performed with the system software (Cell Quest; BD Biosciences).

Apoptosis Analysis. HepG-2 cells were seeded at the density of 2×10^6 cells/mL of the DMEM medium with 10% FBS on 6-well plates to the final volume of 2 mL. The plates

were incubated for overnight and then treated with different concentrations compound **13** for 24 h. Briefly, after treatment with compound **13** for 24 h, cells were collected and washed with PBS twice, and then resuspend cells in 1×Binding Buffer (0.1 M Hepes/NaOH (pH 7.4), 1.4 M NaCl, 25 mM $CaCl_2$) at a concentration of 1×10^6 cells /ml. The cells were subjected to 5 μL of FITC Annexin V (BD, Pharmingen) and 5 μL propidium iodide (PI) staining using annexin-V FITC apoptosis kit followed the 100 μL of the solution was transfer to a 5 mL culture tubeand incubate for 30 min at RT (25 ^{o}C) in the dark. The apoptosis ratio was quantified by system software (Cell Quest; BD Biosciences).

Hoechst 333258 Assay. HepG-2 cells (1×10^6 cells) were seeded in six-well tissue culture platesand exposed todifferentdoses of compound **13** for 24 h. The cells were fixed in 4% paraformaldehyde for 10 min followed by the medium was discarded. The cells were then washed twice with cold PBS and incubated with 0.5 mL of Hoechst 33258 at dark for 5 min. After 5 min incubation, the cells were washed twice with cold PBS and the results were analysis by a Nikon ECLIPSETE2000-S fluorescence microscope using 350 nm excitation and 460 nm emissions.

Determination of Mitochondrial Membrane Potential. HepG-2 cells were seeded at the density of 2×10^6 cells/mL of the DMEM medium with 10% FBS on 6-well plates to the final volume of 2 mL. The plates were incubated for overnight and then treated with compound **13** at different concentrations for 24 h. JC-1 probe was added 20 min after replacing with fresh medium. Cells were collected at 2000 rpm, rinsed twice with cold

PBS and mitochondrial membrane potential was analyzed in FL-1channel by flow cytometer.

ROS Assay. HepG-2 cells were seeded into six-well plates and subjected to various treatments. On the following treatment, cells were collected and washed with PBS twice, and then resuspend cells in 10mM DCFH-DA (Beyotime, Haimen, China) dissolved in cell free medium at 37 ℃ for 30 min in dark, and then washed three times with PBS. Cellular fluorescence was quantified by flow cytometry at an excitation of 485 nm and an emission of 538 nm.

Western Blot Analysis. Total cell lysates from cultured HepG-2 cells after compound **13** treatments as mentioned earlier were obtained by lysing the cells in ice-cold RIPA buffer with protease and phosphatase inhibitor and stored at -20 °C for future use. The protein concentrations were quantified by Bradford method (BIO-RAD) using Multimode varioskan instrument (Thermo Fischer Scientifics). Equal amounts of protein per lane was applied in 12% SDS polyacrylamide gel for electrophoresis and transferred to polyvinylidine difluoride (PVDF) membrane (Amersham Biosciences). After the membrane was blocked at room temperature for 2 h in blocking solution, primary antibody was added and incubated at 4 ℃ overnight. Bax, Bcl-2, cytochrome c, caspase-9, -3, PARP, cyclin B1, CDK1, p21 and p53 antibodies were purchased from Imgenex, USA. After three TBST washes, the membrane was incubated with corresponding horseradish peroxidase-labeled secondary antibody (1:2000) (Santa Cruz) at room temperature for 1 h. Membranes were washed with TBST three times for 15 min and the protein blots were

detected with chemiluminescence reagent (Thermo Fischer Scientifics Ltd.). The X-ray films were developed with developer and fixed with fixer solution.

Antitumor Activity in Vivo. The in vivo cytotoxic activity of complex **13** was investigated using a human hepatocellular carcinoma cell line in BALB/c nude mice. Five week-old female BALB/c nude mice (16−18 g) were housed purchased from Shanghai Ling Chang biotechnology company (China), tumors were induced by a subcutaneous injection in their dorsal region of 10^7 cells in 100 μL of sterile PBS. Animals were randomly divided into six groups, and starting on the second day. When the tumors reached a volume of 100−150 mm^3 in all mice on day 14, the first group was injected with an equivalent volume of 5% dextrose injection via a tail vein injection as the vehicle control mice. No.2 and No.3 groups were treated with cisplatin and CA-4 at the doses of 5 mg/kg body weight once a week for three weeks, respectively. No.4 and No.5 groups were treated with complex **13** at the doses of 5 or 10 mg/kg body weight once a week for three weeks, respectively. The sixth group was treated with cisplatin at the doses of 5 mg/kg body weight combined with CA-4 at the doses of 5 mg/kg body weight once a week for three weeks. All compounds were dissolved in vehicle. Tumor volume and body weights were recorded every other day after drug treatment. All mice were sacrificed after three weeks of treatment and the tumor volumes were measured with electronic digital calipers and determined by measuring length (A) and width (B) to calculate volume ($V = AB^2/2$).

ⓢ**Supporting Information.** The binding modes of complexes **13**, **15** and **9** in the

colchicine binding site of tubulin were carried out using Sybyl-X 2.0 on a windows workstation and ^{1}H NMR, ^{13}C NMR and HR-MS of the target compounds. This material is available free of charge via the Internet at http://pubs.acs.org.

AUTHOR INFORMATION

Corresponding Author

*E-mail: sgou@seu.edu.cn.

*E-mail: whengshan@163.com (H. Wang)

Author Contributions

// Xiaochao Huang and Rizhen Huang contributed equally to this work.

Notes

The authors declare no competing financial interest.

ACKNOWLEDGEMENTS

We are grateful to the National Natural Science Foundation of China (Grant No. 21571033) and the New Drug Creation Project of the National Science and Technology Major Foundation of China (Grant No. 2015ZX09101032) for financial aids to this work. The authors would also like to thank the Fundamental Research Funds for the Central Universities (Project 2242013K30011) for supplying basic facilities to Jiangsu Province Hi-Tech Key Laboratory for Biomedical Research. We also want to express our gratitude to the Priority Academic Program Development of Jiangsu Higher Education Institutions for the construction of fundamental facilities (Project 1107047002). KeyGen Biotech

Company was appreciated for completing the in vivo tests.

REFERENCES

1. Rosenberg, B., VanCamp, L., Trosko, J. E., Mansour, V. H. (1969) Platinum Compounds: a New Class of Potent Anti-tumor Agents. *Nature 222*, 385−386.

2. Kelland, L. (2007) The Resurgence of Platinum-Based Cancer Chemotherapy. *Nature Rev. Cancer 7*, 573−584.

3. Wang, X. Y., Wang, X. H., Guo, Z. J. (2015) Functionalization of Platinum Complexes for Biomedical Applications. *Acc. Chem. Res. 48*, 2622−2631.

4. Liu, F. F., Gou, S. H., Chen, F. H., Fang, L., Zhao, J. (2015) Study on Antitumor Platinum(II) Complexes of Chiral Diamines with Dicyclic Species as Steric Hindrance. *J. Med. Chem. 58*, 6368–6377.

5. Graf, N., Lippard, S. J. (2012) Redox Activation of Metal-based Pro-drugs as a Strategy for Drug Delivery. *Adv. Drug Delivery Rev. 64*, 993–1004.

6. Wilson, J. J., Lippard, S. J. (2012) In Vitro Anticancer Activity of cis-diammineplatinum(II) Complexes with β-diketonate Leaving Group Ligands. *J. Med. Chem*. *55*, 5326–5336.

7. Fuertes, M. A., Alonso, C., Perez, J. M. (2003) Biochemical Modulation of Cisplatin Mechanisms of Action: Enhancement of Antitumor Activity and Circumvention of Drug Resistance. *Chem. Rev. 103*, 645−662.

8. Zhang, W., Shen, J. L., Su, H., Mu, G., Sun, J.-H., Tan, C.-P., Liang, X.-J., Ji, L.-N.,

Mao, Z.-W. (2016) Co-Delivery of Cisplatin Prodrug and Chlorin e6 by Mesoporous Silica Nanoparticles for Chemo-Photodynamic Combination Therapy to Combat Drug Resistance. *ACS Appl. Mater. Interfaces. 8*, 13332–13340.

9. Galanski, M., Jakupec, M. A., Keppler, B. K. (2005) Update of the Preclinical Situation of Anticancer Platinum Complexes: Novel Design Strategies and Innovative Analytical Approaches. *Curr. Med. Chem. 12*, 2075−2094.

10. Mukherjea, D., Rybak, L. P., Sheehan, K. E., Kaur, T., Ramkumar, V., Jajoo, S., Sheth, S. (2011) The Design and Screening of Drugs to Prevent Acquired Sensorineural Hearing Loss. *Expert. Opin. Drug Saf. 6*, 491-505.

11. Wang, D., Lippard, S. J. (2005) Cellular Processing of Platinum Anticancer Drugs. *Nat. Rev. Drug. Discov. 4*, 307-320.

12. Pichler, V., Mayr, J., Heffeter, P., Domotor, O., Enyedy, E. A., Hermann, G., Groza, D., Kollensperger, G., Galanksi, M., Berger, W., et al. (2013) Maleimide-Functionalised Platinum (IV) Complexes as a Synthetic Platform for Targeted Drug Delivery. *Chem. Commun. 49*, 2249-2251.

13. Chin, C. F., Yap, S. Q., Li, J., Pastorin, G., Ang, W. H. (2014) Ratiometric Delivery of Cisplatin and Doxorubicin Using Tumor-Targeting Carbon-Nanotubes Entrapping Platinum(IV) Pro-drugs. *Chem. Sci. 5*, 2265−2270.

14. Yuan, Y. Y., Kwok, R. T. K., Tang, B. Z., Liu, B. (2014) Targeted Theranostic Platinum(IV) Pro-drug with a Built-In Aggregation Induced Emission Light-Up Apoptosis Sensor for Noninvasive Early Evaluation of Its Therapeutic Responses in Situ.

J. Am. Chem. Soc. 136, 2546−2554.

15. Varbanov, H. P., Göschl, S., Heffeter, P., Theiner, S., Roller, A., Jensen, F., Jakupec, M. A., Berger, W., Galanski, M., Keppler, B. K. (2014) A Novel Class of Bis- and Tris-Chelate Diam(m) ine bis(dicarboxylato) Platinum (IV) Complexes as Potential Anticancer Pro-drugs. *J. Med. Chem. 57*, 6751−6764.

16. Peyrot, V., Briand, C., Momburg, R., Sari, J. C. (1986) In vitro Mechanism Study of Microtubule Assembly Inhibition by cis-dichlorodiammine-platinum (II). *Biochem. Pharmacol. 35*, 371−375.

17. Coderch, C., Morreale, A., Gago, F. (2012) Tubulin-Based Structure-Affinity Relationships for Anti-mitotic Vinca Alkaloids. *Anti-Cancer Agent. Med. 12*, 219−225.

18. Bedard, P. L., Di Leo, A., Piccart-Gebhart, M. J. (2010) Taxanes: Optimizing Adjuvant Chemotherapy for Early-Stage Breast Cancer. *Nat. Rev. Clin. Oncol*. *7*, 22–36.

19. Manneville, E. S. (2010) From Signaling Pathways to Microtubule Dynamics: the Key Players. *Curr. Opin. Cell. Biol. 22*, 104–111.

20. Jordan, M. A., Wilson, L. (2004) Microtubules as a Target for Anticancer Drugs. *Nat. Rev. Cancer. 4*, 253–265.

21. Kavallaris, M. (2010) Microtubules and Resistance to Tubulin-Binding Agents. *Nat. Rev. Cancer. 10*, 194−204.

22. Dark, G. G., Hill, S. A., Prise, V. E., Tozer, G. M., Pettit, G. R., Chaplin, D. J. (1997) Combretastatin A-4, an Agent that Displays Potent and Selective Toxicity Toward Tumor Vasculature. *Cancer Res. 57*, 1829−1834.

23. Romagnoli, R., Baraldi, P. G., Salvador, M. K., Preti, D., Tabrizi, M. A., Brancale, A., Fu, X. H., Li, J., Zhang, S. Z., Hamel, E., et al. (2012) Synthesis and Evaluation of 1, 5-disubstituted Tetrazoles as Rigid Analogues of Combretastatin A-4 with Potent Anti-proliferative and Anti-tumor Activity. *J. Med. Chem. 55*, 475−488.

24. Schobert, R., Biersack, B., Dietrich, A., Effenberger, K., Knauer, S., Mueller, T. (2010) 4-(3-Halo/amino-4,5-dimethoxyphenyl)-5-aryloxazoles and -N-methylimidazoles that are Cytotoxic Against Combretastatin A Resistant Tumor Cells and Vascular Disrupting in a Cisplatin Resistant Germ Cell Tumor Model. *J. Med. Chem. 53*, 6595–6602.

25. Chen, H., Li, Y. M., Sheng, C. Q., Lv, Z. L., Dong, G. Q., Wang, T. T., Liu, J., Zhang, M. F., Li, L. Z., Zhang, T., et al. (2013) Design and Synthesis of Cyclopropylamide Analogues of Combretastatin-A4 as Novel Microtubule-Stabilizing Agents. *J. Med. Chem. 56*, 685−699.

26. Yan, J., Pang, Y. Q., Sheng, J. F., Wang, Y. L., Chen, J., Hu, J. H., Huang, L., Li, X. S. (2015) A Novel Synthetic Compound Exerts Effective Anti-tumor Activity in Vivo Via the Inhibition of Tubulin Polymerisation in A549 Cells. *Biochem. Pharmaco. 97*, 51−61.

27. Schobert, R., Biersack, B., Dietrich, A., Knauer, S., Zoldakova, M., Fruehauf, A., Mueller, T. (2009) Pt(II) Complexes of a Combretastatin A-4 Analogous Chalcone: Effects of Conjugation on Cytotoxicity, Tumor Specificity, and Long-Term Tumor Growth Suppression. *J. Med. Chem. 52*, 241−246.

28. Ma, L. L., Ma, R., Wang, Y. P., Zhu, X. Y., Zhang, J. L., Chan, H. C., Chen, X. F., Zhang, W. J., Chiu, S. K., Zhu, G. Y. (2015) Chalcoplatin, a Dual-Targeting and p53

Activator Containing Anticancer Platinum(IV) Pro-drug with Unique Mode of Action. *Chem. Commun. 51*, 6301−6304.

29. Raveendran, R., Braude, J. P., Wexselblatt, E., Novohradsky, V., Stuchlikova, O., Brabec, V., Gandin, V., Gibson, D. (2016) Pt(IV) Derivatives of Cisplatin and Oxaliplatin with Phenylbutyrate Axial Ligands are Potent Cytotoxic Agents that Act by Several Mechanisms of Action. *Chem. Sci. 7*, 2381−2391.

30. Pathak, R. K., Marrache, S., Choi, J. H., Berding, T. B., Dhar, S. (2014) The Pro-drug Platin-A: Simultaneous Release of Cisplatin and Aspirin. *Angew. Chem. Int. Ed. 53*, 1963-1967.

31. Nam, N. H. (2003) Combretastatin A-4 Analogues as Anti-mitotic Antitumor Agents. *Curr. Med. Chem. 10*, 1697−1722.

32. Hsieh, H., Liou, J., Mahindroo, N. (2005) Pharmaceutical Design of Anti-mitotic Agents Based on Combretastatins. *Curr. Pharm. Des*. *11*, 1655−1677.

33. Pettit, G. R., Grealish, M. P., Jung, M. K., Hamel, E., Pettit, R. K., Chapuis, J. C., Schmidt, J. M. (2002) Antineoplastic Agents. 465. Structural Modification of Resveratrol: Sodium Resverastatin Phosphate. *J. Med. Chem. 45*, 2534−2542.

34. Pettit, G. R., Rhodes, M. R., Herald, D. L., Hamel, E., Schmidt, J. M., Pettit, R. K., (2005) Antineoplastic Agents. 445. Synthesis and Evaluation of Structural Modifications of (*Z*)- and (*E*)-Combretastatin A-4. *J. Med. Chem. 48,* 4087−4099.

35. Kamal, A., Mallareddy, A., Ramaiah, M. J., Pushpavalli, S. N. C. V. L., Suresh, P., Kishor, C., Murty, J. N. S. R. C. N., Rao, S., Ghosh, S., Addlagatta, A., Pal-Bhadra, M.

(2012) Synthesis and Biological Evaluation of Combretastatin-Amidobenzothiazole Conjugates as Potential Anticancer Agents. *Eur. J. Med. Chem*. *56*, 166−178.

36. Ravera, M., Gabano, E., Pelosi, G., Fregonese, F., Tinello, S., Osella, D. (2014) A New Entry to Asymmetric Platinum(IV) Complexes via Oxidative Chlorination. *Inorg. Chem. 53*, 9326−9335.

37. Chaudhary, V., Venghateri, J. B., Dhaked, H. P. S., Bhoyar, A. S., Guchhait, S. K., Panda, D. (2016) Novel Combretastatin-2-aminoimidazole Analogues as Potent Tubulin Assembly Inhibitors: Exploration of Unique Pharmacophoric Impact of Bridging Skeleton and Aryl Moiety. *J. Med. Chem*. *59*, 3439−345.

38. Jackman, M., Lindon, C., Nigg, E. A., Pines, J. (2003) Active cyclin B1-Cdk1 first Appears on Centrosomes in Prophase. *Nat. Cell Biol. 5*, 143−148.

39. Papazisis, K. T., Zambouli, D., Kimoundri, O. T., Papadakis, E. S., Vala, V., Geromichalos, G. D., Voyatzi, S., Markala, D., Destouni, E., Boutis, L., et al. (2000) Protein Tyrosine Kinase Inhibitor, Genistein, Enhances Apoptosis and Cell Cycle Arrest in K562 Cells Treated with γ-Irradiation. *Cancer Letters*. *160*, 107−113.

40. Li, Y., Zhang, L. P., Dai, F., Yan, W. J., Wang, H. B., Tu, Z. S., Zhou, B. (2015) Hexamethoxylated Monocarbonyl Analogues of Curcumin Cause G2/M Cell Cycle Arrest in NCI-H460 Cells via Michael Acceptor Dependent Redox Intervention. *J. Agric. Food Chem. 63*, 7731−7742.

41. Wang, J., Yi, J. (2008) Cancer cell killing via ROS: To Increase or Decrease, That is the Question. *Cancer Biol. Ther*. *7*, 1875−1884.

42. Chu, Y. L., Ho, C. T., Chung, J. G., Raghu, R., Lo, Y. C., Sheen, L. Y. (2013) Allicin Induces Anti-human Liver Cancer Cells through the p53 Gene Modulating Apoptosis and Autophagy. *J. Agric. Food Chem. 61*, 9839−9848.

43. Zhang, S. S., Nie, S. P., Huang, D. F., Feng, Y. L., Xie, M. Y. (2014) A Novel Polysaccharide from Ganoderma atrum Exerts Antitumor Activity by Activating Mitochondria-Mediated Apoptotic Pathway and Boosting the Immune System. *J. Agric. Food Chem. 62*, 1581−1589.

44. Ly, J. D., Grubb, D. R., Lawen, A. (2003) The mitochondrial membrane potential (Δψm) in apoptosis: an update. *Apoptosis. 8*, 115−128.

45. Green, D. R., Kroemer, G. (2005) The Pathophysiology of Mitochondrial Cell Death. *Science 305*, 626−629.

46. Fang, Z. X., Liao, P. C., Yang, Y. L., Yang, F. L., Chen, Y. L., Lam, Y. L., Hua, K. F., Wu, S. H. (2010) Synthesis and Biological Evaluation of Polyenylpyrrole Derivatives as Anticancer Agents Acting through Caspases-Dependent Apoptosis. *J. Med. Chem. 53*, 7967–7978.

47. Hsiao, P. C., Hsieh, Y. H., Chow, J. M., Yang, S. F., Hsiao, M., Hua, K. T., Lin, C. H., Chen, H.Y., Chien, M. H. Hispolon Induces Apoptosis through JNK1/2-Mediated Activation of a Caspase-8, -9, and -3-Dependent Pathway in Acute Myeloid Leukemia (AML) Cells and Inhibits AML Xenograft Tumor Growth in Vivo. *J. Agric. Food Chem. 61*, 10063−10073.

48. Kang, K., Song, D. G., Lee, E. H., Lee, K. M., Park, Y. G., Jung, S. H., Pan, C. H.,

Nho, C. W. (2014) Secretome Profiling Reveals the Signaling Molecules of Apoptotic HCT116 Cells Induced by the Dietary Polyacetylene Gymnasterkoreayne B. *J. Agric. Food Chem*. *62*, 2353−2363.

49. Bose, J. S., Gangan, V., Prakash, R., Jain, S. K., Manna, S. K. (2009) A Dihydrobenzofuran Lignan Induces Cell Death by Modulating Mitochondrial Pathway and G2/M Cell Cycle Arrest. *J. Med. Chem. 52,* 3184–3190.

50. Jordan, M. A., Wilson, L. (2004) Microtubules as a Target for Anticancer Drugs. *Nat. Rev. Cancer* 4, 253−265.

51. Schofield, A. V., Gamell, C., Suryadinata, R., Sarcevic, B., Bernard, O. (2013) Tubulin Polymerization Promoting Protein 1 (Tppp1) Phosphorylation by Rho-associated Coiled-coil Kinase (Rock) and Cyclin-dependent Kinase 1 (Cdk1) Inhibits Microtubule Dynamics to Increase Cell Proliferation. *J. Biol. Chem. 288*, 7907-7917.

52. Schiff, P. B., Fant, J., Horwitz, S. B. (1979) Promotion of Microtubule Assembly in Vitro by Paclitaxel. *Nature 227*, 665−667.

53. Liu, Y. N., Wang, J. J., Ji, Y. T., Zhao, G. D., Tang, L. Q., Zhang, C. M., Guo, X. L., Liu, Z.P. (2016) Design, Synthesis, and Biological Evaluation of 1-Methyl-1,4-dihydroindeno[1,2-c] pyrazole Analogues as Potential Anticancer Agents Targeting Tubulin Colchicine Binding Site. *J. Med. Chem.* 59, 5341−5355.

54. Li, C. M., Lu, Y., Ahn, S., Narayanan, R., Miller, D. D., Dalton, J.T. (2010) Competitive Mass Spectrometry Binding Assay for Characterization of Three Binding Sites of Tubulin. *J. Mass. Spectrom.* 45, 1160−1166.

55. Verdier-Pinard, P., Lai, J.-Y., Yoo, H.-D., Yu, J., Marquez, B., Nagle, D. G., Nambu, M., White, J. D., Falck, J. R., Gerwick, W. H., et al. (1998) Structureactivity Analysis of the Interaction of Curacin A, the Potent Colchicines Site Anti-mitotic agent, with Tubulin and Effects of Analogs on the Growth of MCF-7 Breast Cancer Cells. Mol. Pharmacol. 53, 62−67.

56. Wang, G. C., Peng, F., Cao, D., Yang, Z., Han, X. L., Liu, J., Wu, W. S., He, L., Ma, L., Chen, J. Y., et al. (2013) Design, Synthesis and Biological Evaluation of Millepachine Derivatives as a New Class of Tubulin Polymerization Inhibitors. *Bioorg. Med. Chem. 21*, 6844–6854.

57. Yang, Z., Wu, W. S., Wang, J. J., Liu, Li., Li, L. Y., Yang, J. H., Wang, G. C., Cao, D., Zhang, R. H., Tang, M. H., et al. (2014) Synthesis and Biological Evaluation of Novel Millepachine Derivatives As a New Class of Tubulin Polymerization Inhibitors. *J. Med. Chem. 57*, 7977−7989.